

# Dispersion in the large-deviation regime. Part I: shear flows and periodic flows

P. H. Haynes<sup>1</sup> and J. Vanneste<sup>2†</sup>

<sup>1</sup>Department of Applied Mathematics and Theoretical Physics, University of Cambridge,  
Wilberforce Road, Cambridge CB3 0WA, UK

<sup>2</sup>School of Mathematics and Maxwell Institute for Mathematical Sciences, University of  
Edinburgh, King's Buildings, Edinburgh EH9 3JZ, UK

(Received 10 November 2018)

The dispersion of a passive scalar in a fluid through the combined action of advection and molecular diffusion is often described as a diffusive process, with an effective diffusivity that is enhanced compared to the molecular value. However, this description fails to capture the tails of the scalar concentration distribution in initial-value problems. To remedy this, we develop a large-deviation theory of scalar dispersion that provides an approximation to the scalar concentration valid at much larger distances away from the centre of mass, specifically distances that are  $O(t)$  rather than  $O(t^{1/2})$ , where  $t \gg 1$  is the time from the scalar release.

The theory centres on the calculation of a rate function characterising the large-time form of the scalar concentration. This function is deduced from the solution of a one-parameter family of eigenvalue problems which we derive using two alternative approaches, one asymptotic, the other probabilistic. We emphasise the connection between the large-deviation theory and the homogenisation theory that is often used to compute effective diffusivities: a perturbative solution of the eigenvalue problems in the appropriate limit reduces at leading order to the cell problem of homogenisation theory.

We consider two classes of flows in some detail: shear flows and periodic flows with closed streamlines (cellular flows). In both cases, large deviation generalises classical results on effective diffusivity and captures new phenomena relevant to the tails of the scalar distribution. These include approximately finite dispersion speeds arising at large Péclet number  $Pe$  (corresponding to small molecular diffusivity) and, for two-dimensional cellular flows, anisotropic dispersion. Explicit asymptotic results are obtained for shear flows in the limit of large  $Pe$ . (A companion paper, Part II, is devoted to the large- $Pe$  asymptotic treatment of cellular flows.) The predictions of large-deviation theory are compared with Monte Carlo simulations that estimate the tails of concentration accurately using importance sampling.

## 1. Introduction

Taylor (1953) identified the phenomenon of shear dispersion in which a passive scalar, e.g. a chemical pollutant, released in a pipe Poiseuille flow spreads along the pipe according to a diffusion law. The corresponding diffusivity, often termed effective diffusivity to distinguish it from molecular diffusivity, is inversely proportional to molecular diffusivity when the latter is small (see also Aris 1956; Young & Jones 1991). This effective diffusivity is associated with a random walk along the pipe that results from the random

† Email address for correspondence: J.Vanneste@ed.ac.uk

41 sampling of the Poiseuille flow by molecular Brownian motion across the pipe. The dif-  
 42 fusive description of this random walk, and the corresponding Gaussian profile of the  
 43 scalar concentration, of course only apply on time scales that are much longer than the  
 44 Lagrangian correlation time scale.

45 Shear dispersion is a striking example of a broad class of phenomena in which the  
 46 interaction between fluid motion and Brownian motion leads to a strong enhancement of  
 47 dispersion and to effective diffusivities that are orders of magnitude larger than molecular  
 48 diffusivity. The importance of these phenomena in applications, in particular industrial,  
 49 biological and environmental applications, is obvious. This has motivated studies of effec-  
 50 tive diffusivity in many different flows (see Majda & Kramer 1999, for a review). These  
 51 include spatially periodic flows which can be analysed using the method of homogenisa-  
 52 tion. This method, which exploits the separation between the (small) scale of the flow and  
 53 the (large) scale of the scalar field that emerges in the long-time limit, has proved highly  
 54 valuable: it applies to more complicated flows, including time-dependent and random  
 55 flows, and provides a unifying framework for methods used earlier. Shear dispersion, in  
 56 particular, can be regarded as a special case of homogenisation applied to periodic flows,  
 57 where cells repeat in the along pipe direction and the flow in each cell is simple Poiseuille  
 58 flow.

59 In the large literature on shear dispersion, efforts have been made to overcome the re-  
 60 striction to large times that underlies the diffusive approximation, and improved asymp-  
 61 totic estimates that capture some of the early-time behaviour have been obtained (see  
 62 Young & Jones 1991 for a review and Camassa et al. 2010 for more recent results). For  
 63 periodic flows, because the effective diffusivity is more difficult to compute, the focus has  
 64 mainly remained on the derivation of asymptotic estimates and bounds, in particular in  
 65 the limit of small molecular diffusivity (e.g. Majda & Kramer 1999; Novikov et al. 2005).

66 Here we consider a different aspect. The characterisation of dispersion in the long-  
 67 time limit  $t \gg 1$  by an effective diffusivity and hence by a Gaussian scalar distribution  
 68 holds only close to the centre of mass of the distribution: the results of homogenisation  
 69 are in essence a manifestation of the central-limit theorem and apply only to particles  
 70 displaced from the mean by  $O(t^{1/2})$  distances. Our aim is to go beyond this and describe  
 71 the concentration far from the mean. To achieve this, we derive large-deviation estimates  
 72 for the concentration, that is, we derive the rate function  $g$  in an approximation of the  
 73 form  $\exp(-tg(\mathbf{x}/t))$  for the scalar concentration at position  $\mathbf{x}$  and time  $t$ .

74 Large-deviation theory extends the central-limit theorem and applies to numerous  
 75 probabilistic problems (e.g. Dembo & Zeitouni 1998; den Hollander 2000). When ap-  
 76 plied to the stochastic differential equations governing the motion of fluid particles ad-  
 77 vected and diffused in a fluid flow, it naturally yields an improved approximation to the  
 78 scalar concentration (interpreted as a particle-position probability function, cf. Jansons  
 79 & Rogers 1995). This approximation is valid for distances from the mean that are  $O(t)$   
 80 rather than  $O(t^{1/2})$  and therefore captures the tails of the distribution. These are typi-  
 81 cally non-Gaussian and not adequately represented by the diffusive approximation. This  
 82 is illustrated in Figure 1 by the example of dispersion in a plane Couette flow, one of  
 83 the shear flows considered in detail in this paper. The top panel shows the profile along  
 84 the flow of the cross-stream averaged concentration  $C(x, t)$  at four successive times in  
 85 the case of small molecular diffusivity. The figure compares the averaged concentration  
 86 obtained numerically using a Monte Carlo simulation (symbols) with the Gaussian, diffu-  
 87 sive approximation (dashed lines) and the large-deviation approximation derived in §§2–3  
 88 (solid lines). The units of  $x$  and  $t$  have been chosen so that the maximum flow velocity  
 89 and (Taylor) effective diffusivity are both 1. The inadequacy of the diffusive approxima-  
 90 tion in describing the tails of the concentration and the superiority of the large-deviation

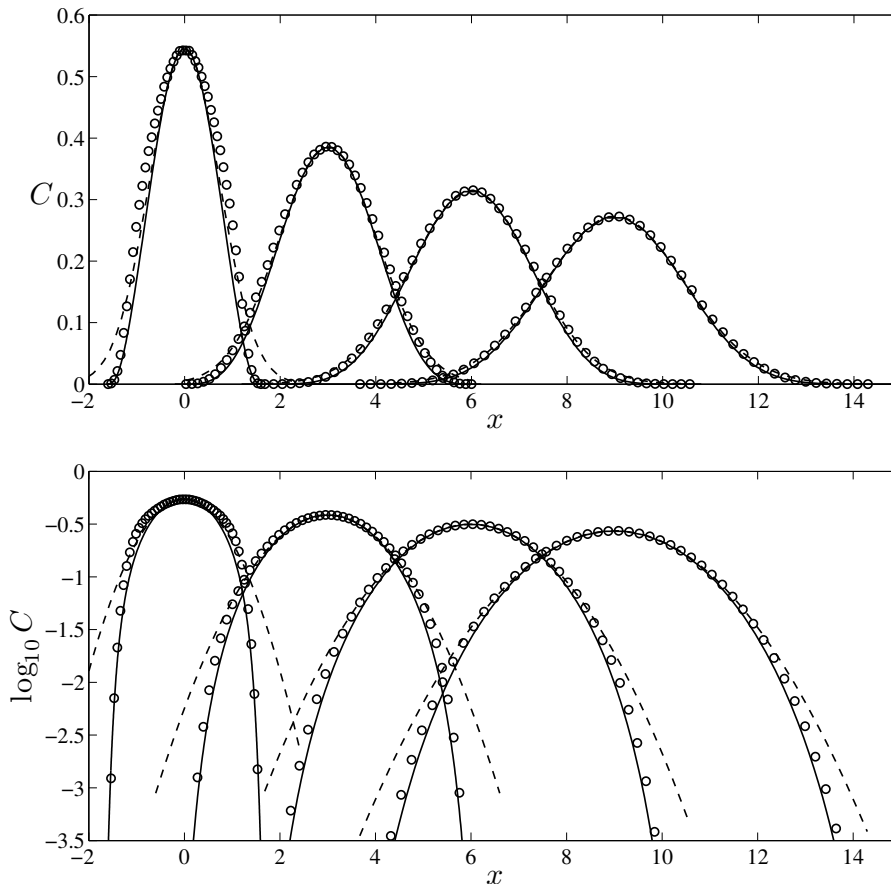


FIGURE 1. Cross-section averaged concentration  $C(x,t)$  (top panel) and its logarithm  $\log_{10} C(x,t)$  (bottom panel) in a Couette flow as a function of  $x$  for  $t = 2, 4, 6$  and  $8$  (from left to right, curves have been offset for clarity). Monte Carlo results (symbols) are compared with the large-deviation and diffusive predictions (solid and dashed lines).

91 approximation are apparent in the top panel for the earliest profile  $C(x, t = 2)$ . They  
 92 are obvious for all the profiles in the bottom panel which displays the results using loga-  
 93 rithmic scale for  $C(x, t)$ . This emphasises the tails of  $C(x, t)$  to reveal how the diffusive  
 94 prediction overestimates dispersion and to demonstrate the effectiveness of the large-  
 95 deviation approximation. We note that while large deviation formally applies for  $t \gg 1$ ,  
 96 it appears here remarkably accurate for moderate  $t$ . (The discrepancies between large-  
 97 deviation and Monte Carlo results for  $t \geq 4$  are mainly attributable to the limitations of  
 98 the straightforward Monte Carlo method used here and are much reduced with the more  
 99 sophisticated methods discussed in §3.)

100 As the Couette-flow example illustrates, large-deviation theory provides estimates of  
 101 the low scalar concentrations in the tails, where the diffusive approximation fails. This  
 102 makes it relevant to a range of applications in which low concentrations matter. Examples  
 103 include the prediction of the first time at which the concentration of a pollutant released  
 104 in the environment exceeds a low safety threshold, and the quantification of the impact  
 105 of stirring on chemical reactions in a fluid. In such examples, there is a strong sensitivity  
 106 of the response (physiological or chemical) to low scalar concentrations that makes the

107 logarithm of the concentration, and hence the rate function  $g$ , highly relevant quantities.  
 108 This broad observation can be made precise for the certain classes of chemical reactions.  
 109 For F-KPP reactions (e.g. Xin 2009), the combination of diffusion and reaction leads to  
 110 the formation of concentration fronts that propagate at a speed that turns out to be  
 111 controlled by the large-deviation statistics of the dispersion and given explicitly in terms  
 112 of the rate function  $g$  (Gärtner & Freidlin 1979; see also Freidlin 1985, Ch. 7, Xin 2009,  
 113 Ch. 2, and Tzella & Vanneste 2014a).

114 The present paper starts in §2 with a relatively general treatment of the large-deviation  
 115 theory of dispersion which applies to time-independent periodic flows and to shear flows.  
 116 The key result is a family of eigenvalue problems parameterised by a variable  $\mathbf{q}$ . The  
 117 principal eigenvalue,  $f(\mathbf{q})$ , is the Legendre transform of the rate function  $g$ . These eigen-  
 118 value problems can be thought of as generalised cell problems in that they resemble and  
 119 extend the cell problem that appears when homogenization is used to compute effective  
 120 diffusivities. In §§2.1–2.2 we present two alternative derivations of the the eigenvalue  
 121 problems: the first is a direct asymptotic method that treats the large-deviation form  
 122 of the concentration as an ansatz (see Kuske & Keller 1997); the second follows the  
 123 standard probabilistic approach based on the Ellis–Gärtner theorem and considers the  
 124 cumulant generating function of the particle position (e.g. Ellis 1995; Dembo & Zeitouni  
 125 1998; den Hollander 2000; Touchette 2009). We then discuss the relation between large  
 126 deviation and homogenisation (§2.3). Homogenisation, and the corresponding diffusive  
 127 approximation, are shown to be recovered when the eigenvalue problems yielding  $f(\mathbf{q})$   
 128 are solved perturbatively for small  $|\mathbf{q}|$  up to  $O(|\mathbf{q}|^3)$  errors. Carrying out the perturba-  
 129 tion expansion to higher orders provides a systematic way of improving on the diffusive  
 130 approximation; in the case of shear dispersion, this recovers earlier results (Mercer &  
 131 Roberts 1990; Young & Jones 1991).

132 The rest of the paper is devoted to dispersion in specific shear and periodic flows.  
 133 We compute the functions  $f$  and  $g$  for the classical Couette and Poiseuille flows in §3  
 134 by solving the relevant one-dimensional eigenvalue problem numerically. We also obtain  
 135 asymptotic results for the concentration at small and large distances from the centre of  
 136 mass. While the first limit recovers the well-known expression for the effective diffusivity  
 137 of shear flows, the second captures the finite propagation speed that exists when diffusion  
 138 along the pipe is neglected. This provides a transparent example of the limitations of the  
 139 diffusive approximation. Section 4 is devoted to a standard example of periodic flow,  
 140 the two-dimensional cellular flow with streamfunction  $\psi = -\sin x \sin y$ . The numerical  
 141 solution of the corresponding eigenvalue problems for specific values of the Péclet number  
 142  $Pe$  (measuring the relative strength of advection and diffusion) reveals interesting features  
 143 of the dispersion, such as anisotropy, that are not captured in the diffusive approximation.  
 144 Using a regular perturbation expansion, we derive explicit results in the limit of small  
 145  $Pe$ . We examine the opposite, large-Péclet-number limit in a companion paper (Haynes  
 146 & Vanneste 2014, hereafter Part II). We conclude the paper with a Discussion in §5.

147 Throughout the present paper and Part II, we verify the predictions of large-deviation  
 148 theory against direct Monte Carlo simulations of particle dispersion. This is not without  
 149 challenges since this requires estimating the tails of distributions which are associated  
 150 with rare events and are, by definition, difficult to sample. We have therefore used im-  
 151 portance sampling and implemented two methods that are applicable broadly. These  
 152 are described in Appendix B. Two other Appendices are devoted to technical details of  
 153 certain asymptotic limits.

## 2. Formulation

We start with the advection–diffusion equation for the concentration  $C(\mathbf{x}, t)$  of a passive scalar. Using a characteristic spatial scale  $a$  as reference length and the corresponding diffusive time scale  $a^2/\kappa$ , where  $\kappa$  is the molecular diffusivity, as a reference time, this equation can be written in the non-dimensional form

$$\partial_t C + \text{Pe} \mathbf{u} \cdot \nabla C = \nabla^2 C, \quad (2.1)$$

where  $\text{Pe} = Ua/\kappa$  is the Péclet number. Here  $U$  is the typical magnitude of the velocity field, which is assumed to be time independent,  $\mathbf{u} = \mathbf{u}(\mathbf{x})$ , and divergence free,  $\nabla \cdot \mathbf{u} = 0$ .

Equation (2.1) can be considered as the Fokker–Planck equation associated with the stochastic differential equation (SDE) which governs the position of fluid particles,

$$d\mathbf{X} = \text{Pe} \mathbf{u}(\mathbf{X})dt + \sqrt{2} d\mathbf{W}, \quad (2.2)$$

where  $\mathbf{W}$  denotes a Brownian motion. In this interpretation and with  $\mathbf{X}(0) = \mathbf{x}_0$ , the initial condition for the concentration is  $C(\mathbf{x}, 0) = \delta(\mathbf{x} - \mathbf{x}_0)$  and the concentration at later times can then be thought of as the transition probability for a particle to move from  $\mathbf{x}_0$  at  $t = 0$  to  $\mathbf{x}$  at  $t$ . We focus on this initial condition and use the notation  $C(\mathbf{x}, t|\mathbf{x}_0)$  when the dependence on  $\mathbf{x}_0$  needs to be made explicit.

In this paper we consider two somewhat different flow configurations. The first, relevant to Taylor dispersion, corresponds to parallel shear flows, with  $\mathbf{u}(\mathbf{x})$  unidirectional and varying in the cross-flow direction only, and a domain that is bounded in this direction. The concentration  $C(\mathbf{x}, t|\mathbf{x}_0)$  then satisfies a no-flux condition at the boundary. The second configuration corresponds to a periodic  $\mathbf{u}(\mathbf{x})$  in an unbounded domain. In both cases, our interest is in the dispersion in the unbounded directions of the domain. The shear-flow configuration can essentially be regarded as a particular case of the more general periodic-flow configuration, with the domain extending over only one period in the streamwise direction and no-flux boundary conditions replacing periodicity conditions. Because of this, we consider the two configurations together when developing the general large-deviation approach in the rest of this section. Any ambiguity that may arise as a result will be clarified in §3 and §4 when we apply the approach separately to shear flows and to two-dimensional periodic flows and obtain explicit results. Mixed configurations, in which the flow is periodic in certain directions and bounded in others, could also be treated with no essential changes.

### 2.1. Large-deviation approximation

We are interested in the form of  $C(\mathbf{x}, t|\mathbf{x}_0)$  for  $t \gg 1$ . Under the assumption that  $|\mathbf{x} - \mathbf{x}_0|/t = O(1)$ , the solution to (2.1) can be sought as the expansion

$$C(\mathbf{x}, t|\mathbf{x}_0) = t^{-d/2} e^{-tg(\boldsymbol{\xi})} (\phi_0(\mathbf{x}, \boldsymbol{\xi}) + t^{-1} \phi_1(\mathbf{x}, \boldsymbol{\xi}) + \dots), \quad \text{where } \boldsymbol{\xi} = (\mathbf{x} - \mathbf{x}_0)/t, \quad (2.3)$$

where  $d$  is the number of spatial dimensions. This can be considered to be a WKB expansion with  $t$  as large parameter. The leading-order approximation

$$C(\mathbf{x}, t|\mathbf{x}_0) \sim t^{-d/2} \phi(\mathbf{x}, \boldsymbol{\xi}) e^{-tg(\boldsymbol{\xi})}, \quad (2.4)$$

has the characteristic large-deviation form in which  $g(\boldsymbol{\xi})$  is the Cramér or rate function (e.g. Dembo & Zeitouni 1998; Touchette 2009, and references therein). The conservation of total mass – the spatial integral of  $C(\mathbf{x}, t|\mathbf{x}_0)$  – imposes that

$$\min_{\boldsymbol{\xi}} g(\boldsymbol{\xi}) = 0 \quad (2.5)$$

191 and explains the presence of the prefactor  $t^{-d/2}$  in (2.4), as an application of Laplace's  
 192 method shows. Note that we concentrate on this leading-order approximation throughout  
 193 and hence omit the subscript 0 from  $\phi$ .

194 Introducing the expansion (2.3) into (2.1) and retaining only the leading order terms  
 195 gives

$$(\boldsymbol{\xi} \cdot \nabla_{\boldsymbol{\xi}} g - g)\phi = \nabla^2 \phi - (\text{Pe} \mathbf{u} + 2\nabla_{\boldsymbol{\xi}} g) \cdot \nabla \phi + (\text{Pe} \mathbf{u} \cdot \nabla_{\boldsymbol{\xi}} g + |\nabla_{\boldsymbol{\xi}} g|^2) \phi. \quad (2.6)$$

196 Letting

$$\mathbf{q} = \nabla_{\boldsymbol{\xi}} g \quad \text{and} \quad f(\mathbf{q}) = \mathbf{q} \cdot \boldsymbol{\xi} - g, \quad (2.7)$$

197 this equation reduces to

$$\nabla^2 \phi - (\text{Pe} \mathbf{u} + 2\mathbf{q}) \cdot \nabla \phi + (\text{Pe} \mathbf{u} \cdot \mathbf{q} + |\mathbf{q}|^2) \phi = f(\mathbf{q})\phi, \quad (2.8)$$

198 where  $\mathbf{q}$  can be regarded as a parameter. This can be rewritten compactly as

$$e^{\mathbf{q} \cdot \mathbf{x}} (\nabla^2 - \text{Pe} \mathbf{u} \cdot \nabla) (e^{-\mathbf{q} \cdot \mathbf{x}} \phi) = f(\mathbf{q})\phi, \quad (2.9)$$

199 in which the form of the operator on the left-hand side makes transparent the connec-  
 200 tion to the advection–diffusion operator  $\nabla^2 - \text{Pe} \mathbf{u} \cdot \nabla$ . The function  $\phi$  satisfies no-flux  
 201 boundary conditions when impermeable boundaries are present or periodic boundary  
 202 conditions in the case of unbounded domains with periodic  $\mathbf{u}(\mathbf{x})$ .

203 Equation (2.8) is central to this paper. Together with its associated boundary condi-  
 204 tions, it gives a family of eigenvalue problems for  $\phi$  parameterised by  $\mathbf{q}$ , with  $f(\mathbf{q})$  as the  
 205 eigenvalue. Solving these eigenvalue problems (numerically in general) provides  $f(\mathbf{q})$  as  
 206 the principal eigenvalue, that is, the eigenvalue with largest real part. The rate function  
 207  $g(\boldsymbol{\xi})$  is then recovered by noting from (2.7) that  $g(\boldsymbol{\xi})$  and  $f(\mathbf{q})$  are related by a Legendre  
 208 transform

$$f(\mathbf{q}) = \sup_{\boldsymbol{\xi}} (\mathbf{q} \cdot \boldsymbol{\xi} - g(\boldsymbol{\xi})) \quad \text{and} \quad g(\boldsymbol{\xi}) = \sup_{\mathbf{q}} (\boldsymbol{\xi} \cdot \mathbf{q} - f(\mathbf{q})). \quad (2.10)$$

209 The fact that the critical points of  $f$  are suprema and the convexity of  $f$  can be deduced  
 210 from the probabilistic interpretation of  $f(\mathbf{q})$  discussed below.† It follows that

$$\boldsymbol{\xi} = \nabla_{\mathbf{q}} f, \quad (2.11)$$

211 which gives a one-to-one map between the parameter  $\mathbf{q}$  and the physical variable  $\boldsymbol{\xi} = \mathbf{x}/t$ .  
 212 The eigenfunction  $\phi$  of (2.8) associated with  $f(\mathbf{q})$  can therefore be equivalently thought  
 213 of as a function of  $\boldsymbol{\xi}$ , as in (2.4), or of  $\mathbf{q}$ , as in (2.8). Note that the maximum principle can  
 214 be used to show that  $f(\mathbf{q})$  is real and that  $\phi$  is sign definite (e.g. Berestycki et al. 1994).  
 215 This is consistent with the asymptotics (2.4) and the observation that the concentration  
 216  $C(\mathbf{x}, t | \mathbf{x}_0)$  is positive for all time if it is initially positive.

217 To summarise, solving the eigenvalue problem (2.8) for arbitrary  $\mathbf{q}$  and performing  
 218 a Legendre transform of the principal eigenvalue yields the large- $t$  approximation (2.4)  
 219 of the concentration. This approximation is valid for  $|\mathbf{x}| = O(t)$  and thus, as discussed  
 220 below, extends the standard diffusive approximation which requires  $|\mathbf{x}| = O(t^{1/2})$ . The  
 221 eigenvalue problem (2.8) can be thought of as a generalised cell problem since, as dis-  
 222 cussed in §2.3, it generalises the cell problem of homogenisation theory. Bensoussan et  
 223 al. (1989, §4.3.1) derive this eigenvalue problem as part of a Floquet–Bloch theory for  
 224 linear equations with periodic coefficients and term it ‘shifted cell problem’ (see also  
 225 Papanicolaou 1995, §3.6, and §4 below).

† Note that the second equality assumes that  $f$  is differentiable (e.g. Touchette 2009).

## 2.2. Probabilistic derivation

226 An alternative view of the problem considers the moment generating function

$$w(\mathbf{q}, \mathbf{x}, t) = \mathbb{E} e^{\mathbf{q} \cdot \mathbf{X}}, \quad \text{with } \mathbf{X}(0) = \mathbf{x} \quad (2.12)$$

228 for the position of the fluid particles satisfying (2.2). Here  $\mathbb{E}$  denotes the expectation over  
229 the Brownian process in (2.2). The generating function obeys the backward Kolmogorov  
230 equation

$$\partial_t w = \text{Pe } \mathbf{u} \cdot \nabla w + \nabla^2 w, \quad \text{with } w(\mathbf{q}, \mathbf{x}, 0) = e^{\mathbf{q} \cdot \mathbf{x}} \quad (2.13)$$

231 (e.g. Øksendal 1998; Gardiner 2004). A solution can be sought in the form

$$w(\mathbf{q}, \mathbf{x}, t) = e^{\mathbf{q} \cdot \mathbf{x} + f(\mathbf{q})t} \phi^\dagger(\mathbf{q}, \mathbf{x}), \quad (2.14)$$

232 where the function  $f(\mathbf{q})$  remains to be determined but will shortly be identified with that  
233 in (2.7).

234 Introducing (2.14) into (2.13) leads to

$$\nabla^2 \phi^\dagger + (\text{Pe } \mathbf{u} + 2\mathbf{q}) \cdot \nabla \phi^\dagger + (\text{Pe } \mathbf{u} \cdot \mathbf{q} + |\mathbf{q}|^2) \phi^\dagger = f(\mathbf{q}) \phi^\dagger, \quad (2.15)$$

235 with no-flux or periodic boundary conditions. This corresponds to a family of eigenvalue  
236 problems, again parameterised by  $\mathbf{q}$ , which are the adjoints of those in (2.8), and hence  
237 have the same eigenvalues and in particular the same principal eigenvalue  $f(\mathbf{q})$ , justifying  
238 the notation in (2.14). This eigenvalue controls  $w(\mathbf{x}, t)$  for  $t \gg 1$ . As a result, it can  
239 alternatively be defined by

$$f(\mathbf{q}) = \lim_{t \rightarrow \infty} \frac{1}{t} \log \mathbb{E} e^{\mathbf{q} \cdot \mathbf{X}(t)} \quad (2.16)$$

240 and interpreted as the limit as  $t \rightarrow \infty$  of the cumulant generating function scaled by  $t^{-1}$ .  
241 This function is convex by definition.

242 The relationship between the large- $t$  asymptotics of  $C(\mathbf{x}, t | \mathbf{x}_0)$  encoded in  $g(\boldsymbol{\xi})$  and  
243 that of  $w(\mathbf{x}, t)$  can be made obvious. Noting from the definition (2.12) that  $w(\mathbf{x}, t)$  is the  
244 Legendre transform with respect to  $\mathbf{x}'$  of  $C(\mathbf{x}', t | \mathbf{x})$  with  $-\mathbf{q}$  the variable dual to  $\mathbf{x}'$ , we  
245 apply Laplace's method to obtain

$$w(\mathbf{q}, \mathbf{x}, t) = \int e^{\mathbf{q} \cdot \mathbf{x}'} C(\mathbf{x}', t | \mathbf{x}) d\mathbf{x}' \asymp \int e^{t(\mathbf{q} \cdot (\boldsymbol{\xi} + \mathbf{x}/t) - g(\boldsymbol{\xi}))} d\boldsymbol{\xi} \asymp e^{\mathbf{q} \cdot \mathbf{x} + t \sup_{\boldsymbol{\xi}} (\mathbf{q} \cdot \boldsymbol{\xi} - g(\boldsymbol{\xi}))},$$

246 where  $\asymp$  denotes the asymptotic equivalence of the logarithms as  $t \rightarrow \infty$  and we use (2.4)  
247 to write  $C(\mathbf{x}', t | \mathbf{x}) \asymp \exp(-tg((\mathbf{x}' - \mathbf{x})/t))$ .

248 From (2.14) we obtain the first part of (2.10). Under the assumption of differentia-  
249 bility of  $f(\mathbf{q})$ , which ensures that  $g(\boldsymbol{\xi})$  is convex, the second part follows, allowing the  
250 computation of the rate function. The argument used in this subsection, which relies  
251 on Laplace's method to establish a connection between rate function  $g(\boldsymbol{\xi})$  and scaled  
252 cumulant generating function  $f(\mathbf{q})$ , is an instance of the Gärtner–Ellis theorem, a funda-  
253 mental result of large-deviation theory which extends Cramér's treatment of the sum of  
254 independent random numbers (see, e.g., Ellis 1995; Dembo & Zeitouni 1998; Touchette  
255 2009). Rigorous results for a problem very similar to that defined above can be found in  
256 Freidlin (1985, Ch. 7). It may be worth contrasting the large-time ( $t \gg 1$ ) large devia-  
257 tions discussed in this paper, with the small-noise ( $\text{Pe} \gg 1$ ) large deviations developed  
258 by Freidlin & Wentzell (see Freidlin & Wentzell 2012): while for small noise a single  
259 (maximum-likelihood or instanton) trajectory controls the rate function  $g$ , this is not  
260 generally the case for large time. As we discuss in the case of shear flows in §3, it is only  
261 for  $\text{Pe} \gg 1$  and  $|\mathbf{q}|$  sufficiently large that  $g$  can be expressed in terms of single trajectory  
262 and that the two forms of large deviations intersect.

Some properties of  $f(\mathbf{q})$  and  $g(\boldsymbol{\xi})$  are useful to infer properties of the dispersion directly from  $f(\mathbf{q})$  without the need to carry out the Legendre transform explicitly. As noted,  $f(\mathbf{q})$  and  $g(\boldsymbol{\xi})$  are convex. Therefore, from (2.11), increasing  $\mathbf{q}$  correspond to increasing  $\boldsymbol{\xi}$ , and  $\mathbf{q}$  can be thought of as a proxy for the more physical variable  $\boldsymbol{\xi}$ . It is clear from (2.16) that  $f(0) = 0$ ; correspondingly,

$$\nabla_{\mathbf{q}} f(0) = \boldsymbol{\xi}_*, \quad (2.17)$$

defines  $\boldsymbol{\xi}_*$  which, by (2.10), minimizes  $g$ . Eq. (2.4) then indicates that the maximum of  $C(\mathbf{x}, t)$  and its centre of mass are located at  $\mathbf{x} \sim \boldsymbol{\xi}_* t$ . Qualitatively the Legendre transform implies that a slow growth of  $f(\mathbf{q})$  away from its minimum corresponds to a rapid growth of  $g(\boldsymbol{\xi})$  and vice versa. In particular, linear asymptotes for  $f(\mathbf{q})$ , say  $f(\mathbf{q}) \sim \lambda q$  as  $q \rightarrow \infty$  in the one-dimensional case, correspond to vertical asymptotes for  $g(\boldsymbol{\xi})$ ,  $g(\boldsymbol{\xi}) \rightarrow \infty$  as  $\boldsymbol{\xi} \rightarrow \lambda^-$ . This implies that  $C(\mathbf{x}, t)$  vanishes for  $x > \lambda t$ , reflecting a finite maximum transport speed for the scalar. Exactly linear asymptotes do not arise for  $f(\mathbf{q})$  because the eigenvalue problem (2.8) for  $|\mathbf{q}| \gg 1$  has the simple solution  $f(\mathbf{q}) \sim |\mathbf{q}|^2$  which corresponds to a purely diffusive behaviour. However, for large Pe, there can be a range of values of  $\mathbf{q}$  for which  $f(\mathbf{q})$  is approximately linear and a finite transport speed controls scalar dispersion.

### 2.3. Relation with homogenisation and its extensions

Much of the literature on scalar dispersion focuses on the computation of an effective diffusivity governing the dispersion for  $t \gg 1$  and  $|\mathbf{x} - \mathbf{x}_0| = O(t^{1/2})$ . In this approximation, (2.1) reduces to the diffusion equation

$$\partial_t C + \text{Pe} \langle \mathbf{u} \rangle \cdot \nabla C = \nabla \cdot (\mathbf{k} \cdot \nabla C), \quad (2.18)$$

where  $\langle \mathbf{u} \rangle$  is the spatial average of  $\mathbf{u}(\mathbf{x})$ , and  $\mathbf{k}$  is an effective diffusivity tensor. Alternatively,  $\langle \mathbf{u} \rangle$  and  $\mathbf{k}$  can be obtained from the particle statistics using

$$\lim_{t \rightarrow \infty} \frac{1}{t} \mathbb{E} \mathbf{X} = \text{Pe} \langle \mathbf{u} \rangle \quad \text{and} \quad \lim_{t \rightarrow \infty} \frac{1}{2t} \mathbb{E} (\mathbf{X} - \text{Pe} \langle \mathbf{u} \rangle t) \otimes (\mathbf{X} - \text{Pe} \langle \mathbf{u} \rangle t) = \mathbf{k}. \quad (2.19)$$

The form of  $\mathbf{k}$  has been derived for a variety of flows using several essentially equivalent methods, starting with Taylor's (1953) work on shear flows. In the last 20 years, homogenisation, as reviewed in Majda & Kramer (1999) and Pavliotis & Stuart (2007), has become the systematic method of choice.

The diffusive approximation (2.18) can be recovered from the more general large deviation results: since the assumption  $|\mathbf{x} - \mathbf{x}_0 - \text{Pe} \langle \mathbf{u} \rangle t| = O(t^{1/2})$  implies that  $\boldsymbol{\xi} \ll 1$  and hence that  $\mathbf{q} \ll 1$ , we can expand  $f(\mathbf{q})$  according to

$$f(\mathbf{q}) = \boldsymbol{\xi}_* \cdot \mathbf{q} + \frac{1}{2} \mathbf{q} \cdot \mathbf{H}_f \cdot \mathbf{q} + O(|\mathbf{q}|^3), \quad (2.20)$$

where  $\mathbf{H}_f$  is the Hessian of  $f$  evaluated at  $\mathbf{q} = 0$ . Taking the Legendre transform gives

$$g(\boldsymbol{\xi}) \sim \frac{1}{2} (\boldsymbol{\xi} - \boldsymbol{\xi}_*) \cdot \mathbf{H}_f^{-1} \cdot (\boldsymbol{\xi} - \boldsymbol{\xi}_*). \quad (2.21)$$

In this approximation the concentration is

$$C(\mathbf{x}, t | \mathbf{x}_0) \asymp e^{-(\mathbf{x} - \boldsymbol{\xi}_* t) \cdot \mathbf{H}_f^{-1} \cdot (\mathbf{x} - \boldsymbol{\xi}_* t) / (2t)} \quad (2.22)$$

corresponding to the solution of (2.18) with

$$\text{Pe} \langle \mathbf{u} \rangle = \boldsymbol{\xi}_* \quad \text{and} \quad \mathbf{k} = \mathbf{H}_f / 2. \quad (2.23)$$

This result also follows from (2.19) noting that the mean and covariances that appear on



the left-hand sides are given by the first and second derivatives with respect to  $\mathbf{q}$  of the cumulant generating function  $\log \mathbb{E} e^{\mathbf{q} \cdot \mathbf{X}} \sim f(\mathbf{q})t$  evaluated  $\mathbf{q} = 0$ .

Since the diffusive approximation is recovered from the large-deviation results by an expansion for small  $\mathbf{q}$ , it can be expected that the method of homogenisation is equivalent to the perturbative solution of the eigenvalue problem (2.8) or (2.15). This is plainly the case. Consider the periodic-flow configuration and assume that  $\langle \mathbf{u} \rangle = 0$  for simplicity. Expanding

$$\phi = 1 + |\mathbf{q}|\phi_1 + |\mathbf{q}|^2\phi_2 + \dots \quad \text{and} \quad f = |\mathbf{q}|\alpha_1 + |\mathbf{q}|^2\alpha_2 + \dots, \quad (2.24)$$

and introducing this into (2.8) yields at  $O(q)$ ,

$$\nabla^2\phi_1 - \text{Pe} \mathbf{u} \cdot \nabla\phi_1 + \text{Pe} \mathbf{u} \cdot \hat{\mathbf{q}} = \alpha_1,$$

where  $\hat{\mathbf{q}} = \mathbf{q}/|\mathbf{q}|$  is a unit vector. Averaging this equation gives that  $\alpha_1 = \text{Pe} \langle \mathbf{u} \cdot \hat{\mathbf{q}} \rangle = 0$ . The solution  $\phi_1$  is then written as

$$\phi_1 = -\hat{\mathbf{q}} \cdot \boldsymbol{\chi}$$

in terms of the periodic, zero-average solution  $\boldsymbol{\chi}$  of the so-called cell problem

$$\nabla^2\boldsymbol{\chi} - \text{Pe} \mathbf{u} \cdot \nabla\boldsymbol{\chi} = \text{Pe} \mathbf{u}. \quad (2.25)$$

(see Majda & Kramer 1999, §2.1). At order  $O(q^2)$ , the eigenvalue problem reduces to

$$\nabla^2\phi_2 - \text{Pe} \mathbf{u} \cdot \nabla\phi_2 - 2\hat{\mathbf{q}} \cdot \nabla\phi_1 + \text{Pe} (\mathbf{u} \cdot \hat{\mathbf{q}})\phi_1 = \alpha_2.$$

Averaging gives

$$\alpha_2 = 1 + \text{Pe} \langle (\mathbf{u} \cdot \hat{\mathbf{q}})\phi_1 \rangle = 1 + \hat{\mathbf{q}}_i \langle \nabla\boldsymbol{\chi}_i \cdot \nabla\boldsymbol{\chi}_j \rangle \hat{\mathbf{q}}_j,$$

where the second equality follows after some manipulations using (2.25) (see Majda & Kramer 1999, p. 251 for details). This corresponds to an effective diffusivity with components

$$\mathbf{k}_{ij} = \frac{1}{2} (H_f)_{ij} = \delta_{ij} + \langle \nabla\boldsymbol{\chi}_i \cdot \nabla\boldsymbol{\chi}_j \rangle,$$

which is the standard homogenisation result. An analogous computation detailed in Appendix A shows how the homogenisation results for shear flows are recovered from the large-deviation calculation.

The perturbative solution of the eigenvalue problem (2.8) offers a route for the systematic improvement of the diffusive approximation. Such improvements, which have been derived for shear flows by Chatwin (1970, 1972), Mercer & Roberts (1990) and others (see Young & Jones 1991, for a review), extend the diffusion equation (2.18) to include higher-order spatial derivatives and increase the accuracy of the approximation for  $t \gg 1$ . They lead to effective equations of the form

$$\partial_t C + \text{Pe} \langle \mathbf{u} \rangle \nabla \cdot C = \mathbf{k}_{ij} \partial_{ij} C + \mathbf{k}_{ijk}^{(3)} \partial_{ijk} C + \mathbf{k}_{ijkl}^{(4)} \partial_{ijkl} C + \dots, \quad (2.26)$$

where summation over repeated indices is understood and we have introduced higher-order effective tensors  $\mathbf{k}_{ijk}^{(3)}$ , etc. The behaviour of the large-deviation function  $f(\mathbf{q})$  as  $\mathbf{q} \rightarrow 0$  encodes all these tensors. This can be deduced from the large-deviation form (2.4) of the concentration which implies that  $\partial_t C \sim f(\mathbf{q})C$  and  $\nabla C \sim -\mathbf{q}C$ . Combining these formally leads to the effective equation

$$\partial_t C = f(-\nabla)C. \quad (2.27)$$

Comparison with (2.26) shows that the various effective tensors that appear are given as derivatives of  $f(\mathbf{q})$  at  $\mathbf{q} = 0$ . Hence they can be computed by continuing the perturbative

328 solution of the eigenvalue problem (2.8) to higher orders in  $q$ . This is demonstrated to  
 329  $O(q^3)$  for shear flows in Appendix A.

330 Another kind of improvement captures finite-time effects, specifically the fact that the  
 331 mean and variance of the particle position have  $O(1)$  corrections to their linear growth  
 332 which depend on initial conditions. These corrections have been computed for some shear  
 333 flows (Aris 1956; Mercer & Roberts 1990; Young & Jones 1991) and termed ‘initial dis-  
 334 placement’ and ‘variance deficit’. Although we do not consider them further in what fol-  
 335 lows, it can be noted that Eq. (2.13) for the moment generating function is exact. Its solution  
 336 for finite time can be expressed as a series of the form  $\sum_n A_n(\mathbf{q}) \exp(f_n(\mathbf{q})t) \phi_n^\dagger(\mathbf{x})$ , where  
 337  $f_n(q)$  and  $\phi_n^\dagger(\mathbf{x})$  denote the complete set of eigenvalues and eigenfunctions of (2.15). The  
 338 constants  $A_n(\mathbf{q})$  can be determined from the initial condition of the concentration. It is  
 339 clear, then, that the first 2 terms in the Taylor expansion of  $A_0(\mathbf{q})$ , where the  $n = 0$   
 340 mode corresponds to the eigenvalue  $f_0(\mathbf{q}) = f(\mathbf{q})$ , determine the initial displacement  
 341 and variance deficit; the other eigenvalues  $f_n(\mathbf{q})$ ,  $n \geq 1$  contribute to exponentially small  
 342 corrections.

343 In the rest of the paper, we apply the results of this section to several specific shear and  
 344 periodic flows. We start with the case of shear flows for which the eigenvalue problems  
 345 (2.8) and (2.15) simplify considerably.

### 346 3. Shear flows

347 Consider the advection by a parallel shear flow  $\mathbf{u} = (u(y), 0)$  in two dimensions, in a  
 348 channel of width  $2a$  corresponding to  $-1 \leq y \leq 1$  for the dimensionless coordinate  $y$ .  
 349 Without loss of generality (exploiting a suitable Galilean transformation as necessary)  
 350 the velocity can be assumed to satisfy

$$\langle u \rangle = \frac{1}{2} \int_{-1}^1 u(y) dy = 0. \quad (3.1)$$

351 Because it is the longitudinal dispersion that is of interest, we modify (2.4) and take the  
 352 large-deviation form of the concentration to be

$$C(\mathbf{x}, t) \sim t^{-1/2} \phi(y, \xi) e^{-tg(\xi)}, \quad \text{where } \xi = \text{Pe}^{-1}x/t, \quad (3.2)$$

353 assuming  $\mathbf{x}_0 = 0$ . Similarly, we write the moment generating function as

$$w(q, \mathbf{x}, t) = \mathbb{E} e^{\text{Pe}^{-1}qX} \simeq e^{\text{Pe}^{-1}qx + f(q)t} \phi^\dagger(y). \quad (3.3)$$

354 Note that  $g$  and  $f$  depend only on the longitudinal variables  $\xi$  and  $q$  and that  $\phi$  can  
 355 be taken  $x$ -independent because of the  $x$ -independence of the flow. The factors  $\text{Pe}^{-1}$  are  
 356 introduced in (3.2)–(3.3) for convenience: they lead to a Legendre pair of functions  $f(q)$   
 357 and  $g(\xi)$  that are independent of  $\text{Pe}$  in the limit  $\text{Pe} \rightarrow \infty$ , at least for  $\xi$ ,  $q = O(1)$ . The  
 358 eigenvalue problem (2.8) then reduces to the Schrödinger form

$$\frac{d^2\phi}{dy^2} + (qu(y) + \text{Pe}^{-2}q^2) \phi = f(q)\phi. \quad (3.4)$$

359 This one-dimensional eigenvalue problem is completed by the no-flux boundary conditions

$$\frac{d\phi}{dy}(-1) = \frac{d\phi}{dy}(1) = 0. \quad (3.5)$$

360 Note that the operator in (3.4) is self adjoint and hence the same equation arises for the  
 361 eigenvalue problem (2.15) for  $\phi^\dagger$  associated with the moment generating function. Note

also that (3.4) can be derived more directly using the Feynman–Kac formula. To see this, write (2.2) explicitly as

$$dX = \text{Pe} u(Y)dt + \sqrt{2}dW_1, \quad dY = \sqrt{2}dW_2, \quad (3.6)$$

and note that  $Y(t) = y + \sqrt{2}W_2$ . The generating function (3.3) then becomes

$$w(q, \mathbf{x}, t) = \mathbb{E} e^{q(\text{Pe}^{-1}(x + \sqrt{2}W_1) + \int_0^t u(y + \sqrt{2}W_2) dt')} = e^{\text{Pe}^{-1}qx + \text{Pe}^{-2}q^2t} \mathbb{E} e^{q \int_0^t u(y + \sqrt{2}W_2) dt'}.$$

Using the Feynman–Kac formula (e.g. Øksendal 1998),  $w$  is seen to satisfy

$$\partial_t w = \partial_{yy} w + (qu(y) + \text{Pe}^{-2}q^2)w$$

and hence, for  $t \gg 1$ , to depend on  $t$  as  $w \asymp \exp(f(q)t)$  with  $f(q)$  the principal eigenvalue in (3.4).

Alternatively, (3.4) is obtained when seeking normal-mode solutions of the form  $C(\mathbf{x}, t) = \phi(k, y) \exp(i(kx - \omega t))$  to the advection–diffusion equation (2.1) provided that the identification  $q = ik$  and  $f(q) = -i\omega(k)$  is made. The large-deviation form of  $C$  is then recovered by applying the steepest-descent method to the normal-mode expansion of  $C(x, y, t)$ . The large-deviation approach makes it clear that the saddle point in the  $k$  plane is on the imaginary axis with a purely imaginary associated frequency  $\omega = if(ik)$ .

Below we solve (3.3)–(3.5) numerically for some classical shear flows. Several general remarks can already be made. First, the term proportional to  $\text{Pe}^{-2}$  in (3.4) is associated with longitudinal (molecular) diffusion. For  $q = O(1)$ , it can be neglected for  $\text{Pe} \gg 1$ , leading to the simpler eigenvalue problem

$$\frac{d^2\phi}{dy^2} + qu(y)\phi = f(q)\phi \quad (3.7)$$

which makes clear that  $f(q)$  and hence  $g(\xi)$  are independent of  $\text{Pe}$  in the limit  $\text{Pe} \rightarrow \infty$  with  $q, \xi = O(1)$ . The large-deviation form of  $C(\mathbf{x}, t)$  can be written in terms of dimensional variables  $x_*$  and  $t_*$  as

$$C(\mathbf{x}_*, t_*) \asymp e^{-a^{-2}\kappa t_* g(x_*/(Ut_*))}, \quad (3.8)$$

and its range of validity as  $\kappa t_*/a^2 \gg 1$  and  $x_* = O(Ut_*)$ . In what follows, we mostly concentrate on the limit  $\text{Pe} \rightarrow \infty$  and solve (3.7) rather than (3.4): the effect of the neglected longitudinal diffusion on  $f(q)$  is straightforward, since it simply adds  $\text{Pe}^{-2}q^2$ , but the corresponding change in  $g(\xi)$  is somewhat more complicated. It is nonetheless a simple matter to estimate the size of  $q$  for which the neglect of longitudinal diffusivity ceases to be a good approximation.

Second, the perturbative solution of eigenvalue problem (3.4) for  $|q| \ll 1$ , provides an effective diffusivity as sketched in §2.3. In terms of  $f(q)$ , the dimensional effective diffusivity is expressed from (3.8) as

$$k_* = \frac{a^2 U^2}{2\kappa} f''(0), \quad (3.9)$$

and is inversely proportional to the molecular diffusivity in the limit  $\text{Pe} \rightarrow \infty$ . The perturbative calculation carried out in Appendix A gives

$$\frac{1}{2}f''(0) = \left\langle \left( \int_{-1}^y u(y') dy' \right)^2 \right\rangle. \quad (3.10)$$

and recovers the explicit form of  $k_*$  as obtained using homogenisation (e.g. Majda & Kramer 1999; Camassa et al. 2010). The first of the corrections to the diffusive approx-

394 imation of Mercer & Roberts (1990) and Young & Jones (1991) is also computed in  
395 Appendix A.

396 Third, the asymptotics of (3.7) indicates that  $f(q)$  tends to  $u_{\pm}q$  as  $q \rightarrow \pm\infty$ , where  $u_{\pm}$   
397 denote the maximum and minimum velocities in the channel. This can be seen by noting  
398 that  $f(q)$  is the lowest eigenvalue of a Schrödinger operator which, in the semiclassical  
399 limit  $|q| \rightarrow \infty$ , is given by the minimum of the potential  $qu(y)$  (e.g. Simon 1983). The  
400 implication, as discussed in §2.2, is that  $g(\xi) \rightarrow \infty$  as  $\xi \rightarrow u_{\pm}$ . Physically, this corresponds  
401 to the fact that fluid particles have longitudinal velocities in the range  $[u_-, u_+]$ ; changes  
402 in the concentration therefore propagate at finite speeds and the concentration  $C$  is  
403 compactly supported for  $x_* \in [u_-t_*, u_+t_*]$ . This is only an approximation of course: when  
404 longitudinal molecular diffusion is taken into account, there is no limit on the propagation  
405 speed. It is readily seen that the term  $\text{Pe}^{-2}q^2$  becomes comparable to  $u_{\pm}q$  in  $f(q)$  for  $q =$   
406  $O(\text{Pe}^2)$  and that the rate function is approximately the diffusive  $g(\xi) \sim \text{Pe}^2(\xi - u_{\pm})^2/4$   
407 for  $\xi$  near  $u_+$  ( $u_-$ ) or larger (smaller). This form of  $g$  can also be shown to arise from  
408 an application of the Freidlin & Wentzell (2012) small-noise large-deviation theory and  
409 is controlled by a single maximum-likelihood trajectory. (This applies only when  $q$  is  
410 sufficiently large: the dimensional expression (3.8) makes this clear, with an argument  
411 of the exponential that scales like  $\kappa$  whereas the small-noise large deviation necessarily  
412 leads to a  $\kappa^{-1}$  scaling, corresponding to a  $\text{Pe}^2$  factor with our non-dimensionalisation.)

413 Finally, we note that the eigenfunctions  $\phi(y, \xi)$ , where the  $\xi$  dependence is inferred  
414 from the  $q$ -dependence using  $\xi = f'(q)$ , have a simple interpretation. For  $\xi > 0$  the  
415 amount of scalar at  $y$  for  $x > \xi t$  can be approximated as

$$\int_{\xi t}^{\infty} C(x, y, t) dx \asymp \phi(y, \xi) e^{-tg(\xi)}, \quad (3.11)$$

416 since, by the convexity of  $g$ , the integral is dominated by the contribution of the endpoint  
417  $x = \xi t$ . Therefore  $\phi(y, \xi)$  gives the scalar distribution across the shear flow of particles  
418 with average speed greater than  $\xi > 0$ . Similarly, for  $\xi < 0$ ,  $\phi(y, \xi)$  gives the distribution  
419 of particles with speed less than  $\xi$ .

### 420 3.1. Couette flow

421 We now examine classical shear flows, starting with the plane Couette flow

$$u(y) = y. \quad (3.12)$$

422 The dispersion in this flow is illustrated in Figure 1. The figure shows how the diffusive  
423 and large-deviation approximations provide a good approximation in the core of the  
424 scalar distribution and how only large deviation captures the tails. Figure 1 does not  
425 resolve the tails of  $C(x, t)$  with sufficient detail to assess the validity of the large-deviation  
426 approximation fully, however. In what follows, we test systematically the large-deviation  
427 prediction for  $f(q)$ , defined as

$$f(q) = \lim_{t \rightarrow \infty} \frac{1}{t} \log \mathbb{E} e^{\text{Pe}^{-1}qX(t)} \quad (3.13)$$

428 with our shear-flow scaling, by comparing the value obtained by solving the eigenvalue  
429 problem (3.4) for a range of  $q$  with careful Monte Carlo estimates. The eigenvalue problem  
430 is solved using a finite-difference scheme. (An exact solution can be written in terms  
431 of Airy functions, but it is not particularly illuminating). The Monte Carlo estimates  
432 approximate the right-hand side of (3.13) as an average over a large number of solutions  
433 of (3.6). However, a straightforward implementation does not provide a reliable estimate  
434 for  $f(q)$  except for small values of  $q$ . This is because  $f(q)$  for moderate to large  $q$  is

435 controlled by rare realisations which are not sampled satisfactorily. To remedy this, it is  
 436 essential to use an importance-sampling technique which concentrates the computational  
 437 effort on these realisations. For the results reported in this paper, we have implemented  
 438 a version of Grassberger's (1997) pruning-and-cloning technique which we describe in  
 439 Appendix B.1.

440 Results for the plane Couette flow are displayed in the leftmost panels of Figure 2.  
 441 The top panel shows the eigenvalue and Monte Carlo approximations of  $f(q)$  along with  
 442 asymptotic approximations valid for small and large  $q$ . The small- $q$  approximation for  
 443  $f(q)$  is found from (3.10) as

$$f(q) \sim \frac{2}{15}q^2 \quad \text{as } q \rightarrow 0. \quad (3.14)$$

444 The large- $|q|$  approximation is obtained by noting that for  $q \rightarrow \pm\infty$ , the solution to (3.7)  
 445 is localised in boundary layers near  $y = \pm 1$ . Concentrating on  $q \rightarrow \infty$ , we introduce  
 446  $y = 1 - q^{-1/3}Y$  and  $f(q) = q + q^{2/3}\mu$  into (3.7). To leading order, this gives

$$\frac{d^2\phi}{dY^2} - Y\phi = \mu\phi, \quad (3.15)$$

447 with solution  $\phi = \text{Ai}(Y + \mu)$  decaying as  $Y \rightarrow \infty$ . Imposing the boundary condition at  
 448  $Y = 0$  gives the equation  $\text{Ai}'(\mu) = 0$  for  $\mu$ . Hence we have

$$f(q) \sim |q| - 1.019|q|^{2/3} \quad \text{as } |q| \rightarrow \infty, \quad (3.16)$$

449 using symmetry to deal with  $q \rightarrow -\infty$ .

450 The top left panel of Figure 2 confirms the validity of the eigenvalue calculation and  
 451 of the asymptotic estimates. In the case of the  $|q| \gg 1$  estimates, a constant is added to  
 452 (3.16) to ensure a good match; with this  $o(1)$  correction, the asymptotic formula appears  
 453 to be accurate for  $|q|$  as small as 3, say. The dispersive approximation corresponding  
 454 to the parabola (3.14) overestimates  $f(q)$  for all  $q$ , indicating that this approximation  
 455 overestimates the speed of dispersion or equivalently the magnitude of the tails of the  
 456 distribution.

457 The rate function  $g(\xi)$  is shown in the second row of Figure 2. The solid curve is  
 458 obtained by Legendre transforming the function  $f(q)$  computed by numerical solution  
 459 of the eigenvalue problem. This is compared with direct Monte Carlo estimates. Again,  
 460 it is crucial to use importance sampling to obtain a reliable estimate of  $g(\xi)$  for  $\xi$  not  
 461 small. We have chosen to integrate a modified dynamics in which particles, instead of  
 462 simply diffusing in the  $y$ -direction, also experience of drift towards the wall at  $y = 1$  (or  
 463  $y = -1$ ). A better sampling is obtained because the wall regions control  $g(\xi)$  for large  
 464  $|q|$ ; the method is described in Appendix B.2. The Figure also shows the asymptotic  
 465 approximations for  $g(\xi)$  deduced from (3.14) and (3.16) by Legendre transform and given  
 466 by

$$g(\xi) \sim \frac{15}{8}\xi^2 \quad \text{as } \xi \rightarrow 0 \quad \text{and} \quad g(\xi) \sim \frac{4 \cdot 1.019^3}{27(1 \mp \xi)^2} \quad \text{as } \xi \rightarrow \pm 1. \quad (3.17)$$

467 The match between the values of  $g(\xi)$  derived from the eigenvalue problem and those  
 468 obtained by Monte Carlo sampling provides a direct check on the validity of the large-  
 469 deviation theory. The discrepancy between the exact  $g(\xi)$  and its diffusive approximation  
 470 confirms that diffusion overestimates the dispersion speed, as inferred already from the  
 471 plot of  $f(q)$ . The finite support of the concentration distribution for  $\xi \in [-1, 1]$ , arising  
 472 from the neglect of longitudinal molecular diffusion, is also hinted at by the large slopes of  
 473  $g$  for  $\xi \approx \pm 0.8$ . The large- $|\xi|$  approximation to  $g(\xi)$  (with  $o(1)$  term fixed by inspection)

474 is seen to be accurate for  $|\xi| \geq 0.5$  and could be combined with the small  $\xi$  approximation  
 475 to provide a satisfactory uniform approximation.

476 The third panel on the left of Figure 2 shows the map between  $\xi = f'(q)$  that arises  
 477 as part of the Legendre transform. This identifies the location  $x = \xi t$  which control the  
 478 corresponding exponential moment  $\mathbb{E} \exp(qX)$  for large  $t$ . Finally, the fourth panel shows  
 479 profiles of the eigenfunctions  $\phi(\xi, y)$  of (3.4) for several values of  $q$ . According to (3.11),  
 480 these give the structure of the concentration profile for  $x/t$  larger than  $\xi = f'(q)$ . Thus,  
 481 for instance, the eigenfunction for  $q = 5$  approximately corresponds to  $x/t \geq 0.5$  (see  
 482 third panel). As  $q$  and hence  $\xi$  increase (or decrease) the profile becomes more and more  
 483 localised in the region of maximum (or minimum) velocity, that is, near  $y = 1$  ( $y = -1$ ).  
 484 The eigenfunctions for finite  $q$  are to be contrasted with the standard (homogenisation)  
 485 results on Taylor dispersion which correspond to eigenfunctions that are small,  $O(q)$   
 486 perturbations to the uniform eigenfunction  $\phi = 1$ .

### 487 3.2. Plane Poiseuille flow

488 We next examine the plane Poiseuille flow

$$u(y) = 1/3 - y^2. \quad (3.18)$$

489 The small- $q$  approximation in this case is readily found from (3.10) to be

$$f(q) \sim \frac{8}{945}q^2 \quad \text{as } q \rightarrow 0. \quad (3.19)$$

490 For  $q \gg 1$ , the solution is localised around the maximum of the velocity at  $y = 0$ . For the  
 491 required boundary-layer analysis, we let  $y = q^{-1/4}Y$  and  $f(q) = q/3 + \mu q^{1/2}$  and obtain

$$\frac{d^2\phi}{dY^2} - Y^2\phi = \mu\phi. \quad (3.20)$$

492 The solution corresponding to the largest eigenvalue  $\mu$  is the Gaussian  $v = \exp(-Y^2/2)$ ,  
 493 leading to  $\mu = -1$  and

$$f(q) \sim q/3 - q^{1/2} \quad \text{as } q \rightarrow \infty. \quad (3.21)$$

494 For  $q \ll -1$ , the asymptotic treatment is similar to that of the Couette flow: we let  
 495  $y = 1 - |q|^{1/3}Y$  and  $f(q) = 2|q|/3 + \mu|q|^{2/3}$  and find that  $\phi \sim \text{Ai}(2^{1/3}(Y + \mu/2))$  and  
 496 hence  $\text{Ai}'(2^{-2/3}\mu) = 0$ . This gives the approximation

$$f(q) \sim -2q/3 - 1.617q^{2/3} \quad \text{as } q \rightarrow -\infty. \quad (3.22)$$

497 The corresponding rate function  $g(\xi)$  is derived by Legendre transform, yielding the  
 498 asymptotic behaviours

$$g(\xi) \sim \frac{945}{32}\xi^2 \quad \text{as } \xi \rightarrow 0, \quad (3.23)$$

$$g(\xi) \sim \frac{1}{4(1/3 - \xi)} \quad \text{as } \xi \rightarrow 1/3, \quad \text{and } g(\xi) \sim \frac{4 \cdot 1.617^3}{27(2/3 + \xi)^2} \quad \text{as } \xi \rightarrow -2/3. \quad (3.24)$$

500 The numerical and asymptotic results obtained for the plane Poiseuille flow are dis-  
 501 played in the second column of Figure 2. As for the Couette flow, the diffusive approx-  
 502 imation (3.19) and (3.23) is seen to overestimate the speed of dispersion, leading to an  
 503 overestimate of  $f(q)$  and an underestimate of  $g(\xi)$ . The concentration distribution for the  
 504 Poiseuille flow is skewed, with  $g(\xi)$  increasing faster for  $\xi > 0$  than  $\xi < 0$  corresponding  
 505 to smaller concentrations for  $\xi > 0$  than for  $\xi < 0$ . The eigenfunctions shown in the  
 506 bottom panel illustrate how  $f(q)$  for large  $q$  (small  $q$ ) and hence  $g(\xi)$  for large  $\xi$  (small  $\xi$ )  
 507 are controlled by motion near the centre (periphery) of the flow. This culminates in the

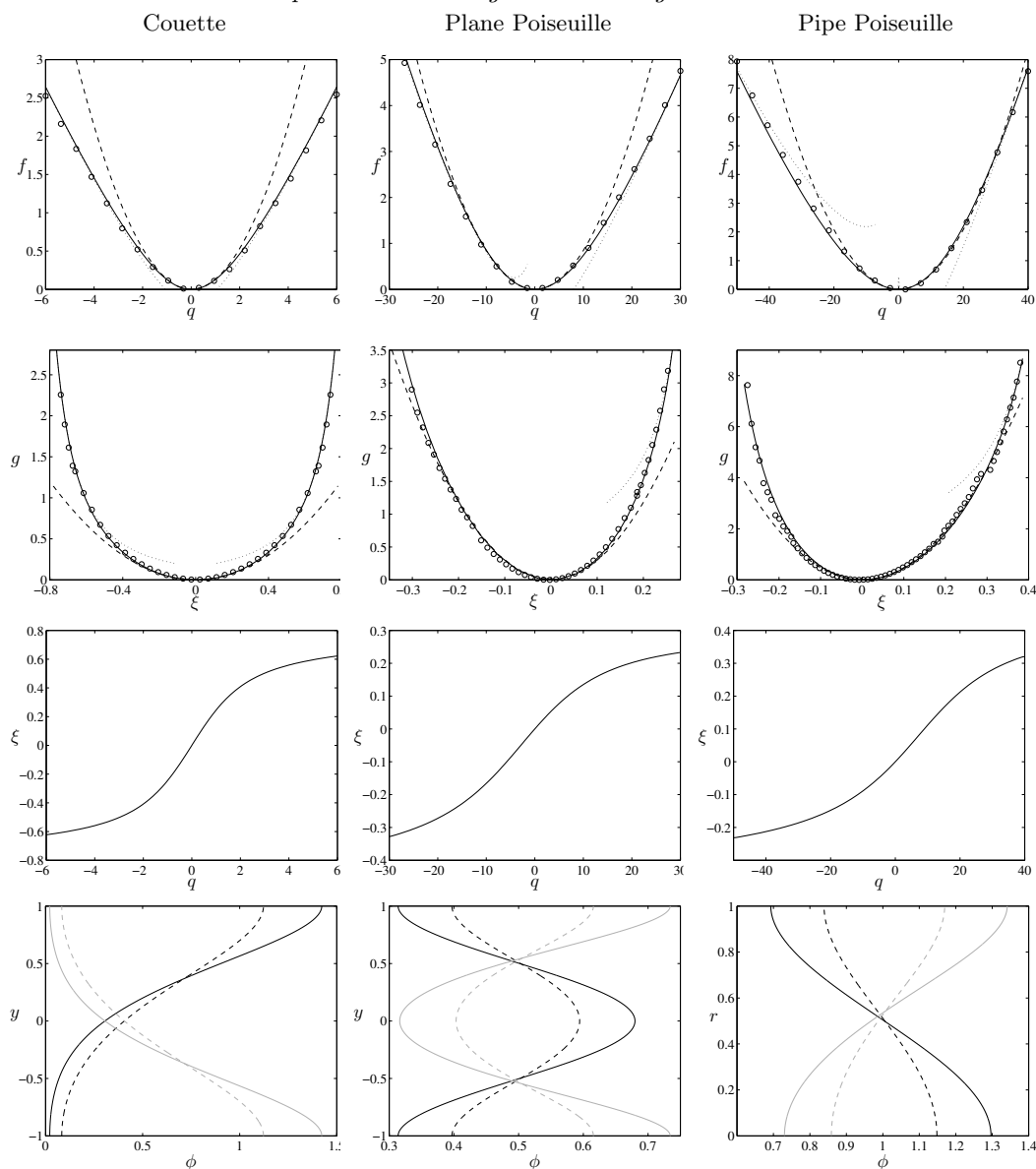


FIGURE 2. Large-deviation results for Couette, plane Poiseuille and pipe Poiseuille flows. First row: the eigenvalue  $f(q)$  obtained by numerical solution of the eigenvalue problem (solid line) is compared with Monte Carlo estimates (symbols). The small- $q$  (diffusive) and large- $q$  asymptotic approximations are also shown (dashed and dotted lines). Second row: the rate function  $g(\xi)$  obtained by Legendre transform of the eigenvalue problem solution  $f(q)$  (solid line) is compared with direct Monte Carlo estimates (symbols). The asymptotic approximations for small  $\xi$  and for  $\xi \rightarrow u_{\pm}$ , the maximum and minimum flow speeds, are also shown (dashed and dotted lines). (For the two Poiseuille flows, the approximations for  $\xi \rightarrow u_{-}$  are not shown because the range of  $\xi$  does not extend to their regions of validity.) Third row: map between  $q$  and  $\xi = x/t$  derived from the numerical estimate of  $f(q)$ . Fourth row: eigenfunctions  $\phi$  for  $q = 5, 10$  (dashed and solid black lines) and for  $q = -5, -10$  (dashed and solid grey lines).

508 limits  $q, \xi \rightarrow \infty$  ( $-\infty$ ) as the boundary-layer form of the eigenfunctions derived above  
509 indicates.

### 510 3.3. Pipe Poiseuille flow

511 We conclude this section by considering the Poiseuille flow in a pipe, with velocity

$$u(r) = 1/2 - r^2, \quad (3.25)$$

512 where  $r = \sqrt{y^2 + z^2}$ . This flow is three-dimensional, with particles diffusing across the  
513 flow in both the  $y$ - and  $z$ -directions. While the eigenfunctions for axisymmetric flows  $\phi$   
514 can in principle depend on  $y$  and  $z$  independently, the principal eigenvalue determining  
515  $f(q)$  is obtained for axisymmetric  $\phi$ :  $\phi = \phi(r)$ . Correspondingly, the eigenvalue problem  
516 (3.7) of plane shear flows is replaced by

$$\frac{1}{r} \frac{d}{dr} \left( r \frac{d\phi}{dr} \right) + qu(r)\phi = f(q)\phi \quad (3.26)$$

517 with boundary conditions  $d\phi/dr = 0$  at  $r = 0, 1$ .

518 The small- $q$ , diffusive approximation  $f(q) \sim \alpha_2 q^2$  for general axisymmetric shear flows  
519 is quoted in Appendix A as (A 6). For the Poiseuille flow, this gives

$$f(q) \sim \frac{1}{192} q^2 \quad \text{as } q \rightarrow 0. \quad (3.27)$$

520 For  $q \gg 1$ , an approximation to  $f(q)$  is derived from (3.26) using a boundary-layer  
521 approach: we let  $r = q^{-1/4} R$  and  $f(q) = q/2 + \mu q^{1/2}$  to find the leading-order equation

$$\frac{1}{R} \frac{d}{dR} \left( R \frac{d\phi}{dR} \right) - R^2 \phi = \mu \phi, \quad (3.28)$$

522 with solution  $\phi = \exp(-R^2/2)$ , corresponding to  $\mu = -2$ . Therefore,

$$f(q) \sim q/2 - 2q^{1/2} \quad \text{as } q \rightarrow \infty. \quad (3.29)$$

523 The analysis for  $q \ll -1$  is almost identical to that carried out for the plane Poiseuille  
524 flow and leads to

$$f(q) \sim -q/2 - 1.617q^{2/3} \quad \text{as } q \rightarrow -\infty. \quad (3.30)$$

525 Computing the Legendre transform of (3.27), (3.29) and (3.30) yields the corresponding  
526 asymptotics results for the rate function, namely

$$g(\xi) \sim 48\xi^2 \quad \text{as } \xi \rightarrow 0, \quad (3.31)$$

527

$$g(\xi) \sim \frac{1}{(1/2 - \xi)} \quad \text{as } \xi \rightarrow 1/2, \quad \text{and } g(\xi) \sim \frac{4 \cdot 1.617^3}{27(1/2 + \xi)^2} \quad \text{as } \xi \rightarrow -1/2. \quad (3.32)$$

528 Note that (3.31) recover's Taylor's original result (Taylor 1953).

529 The numerical and asymptotic results for the pipe Poiseuille flow are shown in the  
530 rightmost panels of Figure 2. The diffusive approximation is seen to mostly overestimate  
531 the dispersion speed, although it turns out to be remarkably accurate for  $q, \xi > 0$ . Close  
532 inspection shows in fact that there is a range of values of  $q, \xi > 0$  for which diffusion  
533 underestimates somewhat the concentration, in contrast to the other cases considered.  
534 Note that the skewness for the pipe Poiseuille flow is opposite to that of the plane  
535 Poiseuille flow, with larger concentrations predicted for  $\xi > 0$  than  $\xi < 0$ .



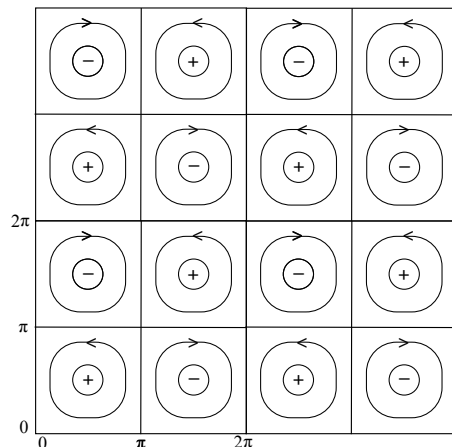
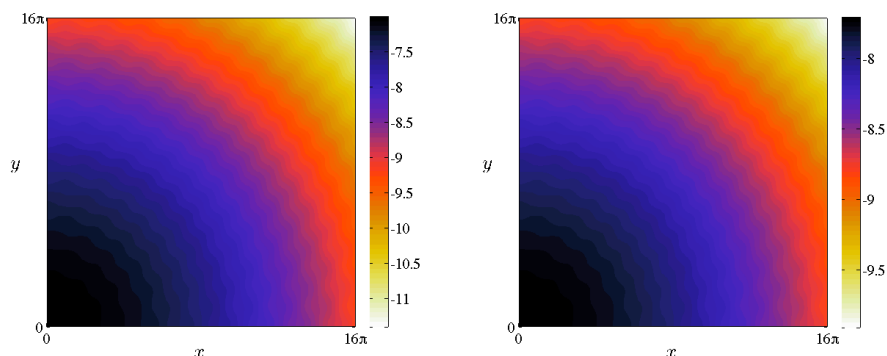


FIGURE 3. Streamlines of the cellular flow (4.1). Four of the periodic cells are shown.

FIGURE 4. (Colour online.) Concentration (in logarithmic scale) at times  $t = 250$  (left) and  $t = 500$  (right) of a scalar initially released in the central cell of a cellular flow with  $Pe = 1$ .

#### 536 4. Periodic flows

537 We now turn to two-dimensional periodic flows. The formalism of § 2 applies directly:  
 538  $f(\mathbf{q})$  is obtained by solving the eigenvalue problem (2.8) with periodic boundary con-  
 539 ditions for  $\phi$ . Eq. (2.8) can also be obtained in an alternative manner: because the  
 540 advection–diffusion equation (2.1) has periodic coefficients, its solutions can be sought in  
 541 the Floquet–Bloch form  $C(\mathbf{x}, t) = \phi(\mathbf{k}, \mathbf{x}) \exp(i(\mathbf{k} \cdot \mathbf{x} - \omega t))$ , which leads to (2.8) with  
 542  $i\mathbf{k} = \mathbf{q}$  and  $\omega(\mathbf{k}) = if(\mathbf{q})$  (Bensoussan et al. 1989; Papanicolaou 1995). This approach  
 543 gives a representation of the concentration as an integral over  $\mathbf{k}$  whose large- $t$  asymp-  
 544 totics, derived using the steepest-descent method, reduces to the large-deviation form  
 545 (2.4).

546 We focus our attention on the cellular flow

$$\mathbf{u}(x, y) = (-\partial_y \psi, \partial_x \psi) \quad \text{with} \quad \psi = -\sin x \sin y. \quad (4.1)$$

547 This flow, with period  $2\pi$  in both the  $x$ - and  $y$ -direction, consists of a regular array of cells  
 548 in which the fluid is rotating alternatively clockwise and counterclockwise along closed  
 549 streamlines; see Figure 3. It has received a great deal of attention, most of it devoted  
 550 to the properties of the effective diffusivity that can be computed by homogenisation,

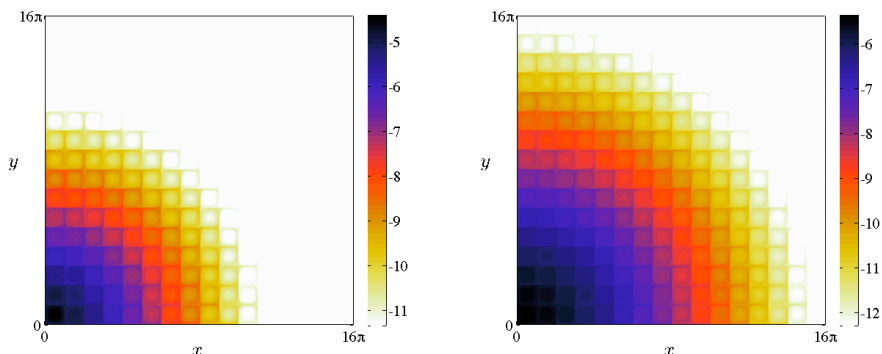


FIGURE 5. (Colour online.) Concentration (in logarithmic scale) at times  $t = 2$  (left) and  $t = 4$  (right) of a scalar released in the central cell of a cellular flow with  $Pe = 250$ .

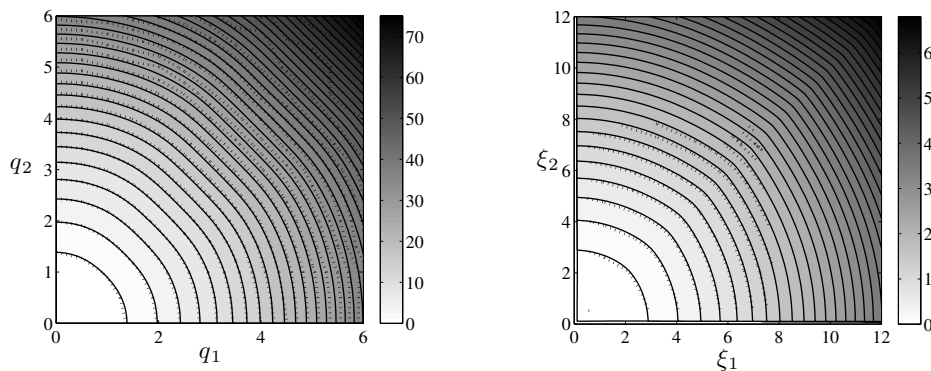


FIGURE 6. Left:  $f$  as a function of  $\mathbf{q}$  for the cellular flow with  $Pe = 1$ . The solid contours and shading have been obtained by solving the eigenvalue problem (2.8) numerically, the dotted contours by Monte Carlo simulations with importance sampling ( $10^5$  realisations for each value of  $\mathbf{q}$ ). Right: corresponding rate function  $g$  as a function of  $\mathbf{q}$  obtained by Legendre transforming the results on the left. Note that the noise in the Monte Carlo results lead to an estimate of  $g$  that is reliable in a restricted range of  $\xi$ .

551 especially in the limit of large Péclet number; see Majda & Kramer (1999, §2) for a  
 552 review, and Novikov et al. (2005) and Gorb et al. (2011) for more recent references.

553 To illustrate the dispersion of a passive scalar in this flow, we show in Figures 4–5 the  
 554 concentration field obtained by solving numerically the advection–diffusion equation (2.1)  
 555 for  $Pe = 1$  and  $Pe = 250$ . Only the first quadrant is shown since the field has a four-fold  
 556 symmetry. For  $Pe = 1$ , molecular diffusion plays a major part across the domain, leading  
 557 to a smooth evolution, with only some modulations in the form of diagonal bands in the  
 558 central sector of the quadrant and of cells located near the coordinate axes. For  $Pe = 250$ ,  
 559 advection dominates, resulting in an apparent finite propagation speed and the obvious  
 560 mark of the flow structure on the scalar field. The importance of the separatrices, around  
 561 which boundary layers of high concentrations are established, is clear. As the distance  
 562 from the origin increases, there is gradual change in the scalar distribution within the  
 563 cells, from almost uniform near the origin to essentially zero at large distance. This  
 564 feature is discussed briefly below and fully elucidated in Part II.

565 Let us now turn to the predictions of large-deviation theory. We have developed a  
 566 code for the numerical solution of the eigenvalue problem (2.8) for (4.1). This relies on

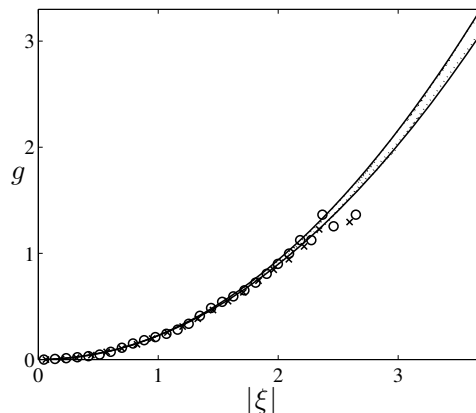


FIGURE 7. Rate function  $g$  as a function of  $|\xi|$  for the cellular flow with  $Pe = 1$ . The curves have been obtained by Legendre transforms of  $f$  computed by solving the eigenvalue problem (solid curves) and Monte Carlo simulation ( $10^4$  realisations for each  $\mathbf{q}$ , dotted curves); the symbols have been obtained from a direct Monte Carlo estimation of the particle position pdf ( $4 \times 10^7$  realisations). The two pairs of curves and two types of symbols correspond to  $\xi = |\xi|(1, 0)$  (steeper curves and circles) and  $\xi = |\xi|(1, 1)/\sqrt{2}$  (shallower curves and squares).

567 a straightforward finite-difference discretisation and on the matlab routine ‘eigs’ for the  
 568 solution of the resulting matrix eigenvalue problem. The convergence of the algorithm  
 569 requires a good first guess for the eigenvalue; since we are interested in obtaining  $f(\mathbf{q})$   
 570 for a range of  $\mathbf{q} = (q_1, q_2)$ , the code performs an iteration over  $q_1$  and  $q_2$ , using at  
 571 each step the previous value of  $f(\mathbf{q})$  as its first guess. Since  $f$  satisfies the obvious  
 572 symmetries  $f(\pm q_1, \pm q_2) = f(q_1, q_2)$ , we concentrate on the first quadrant of the  $\mathbf{q}$ -plane.  
 573 The symmetry  $f(q_1, q_2) = f(q_2, q_1)$  can also be exploited.

574 The left panel of Figure 6 shows the numerical approximation to  $f$  obtained using  
 575 this code for  $Pe = 1$ . It is compared with the result of a Monte Carlo estimate which  
 576 relies on the importance-sampling algorithm described in Appendix B.1. In addition  
 577 to confirming the validity of the large-deviation approximation and of the numerical  
 578 implementation, the figure illustrates general qualitative features of  $f$ . For small  $|\mathbf{q}|$ ,  $f$   
 579 is approximately isotropic, consistent with the result of homogenisation theory which  
 580 predicts a diagonal effective diffusivity tensor. For  $|\mathbf{q}|$  of order-one or larger, however,  
 581  $f$  is anisotropic, taking smaller values along the axes  $\mathbf{q} = |\mathbf{q}|(1, 0)$  and  $\mathbf{q} = |\mathbf{q}|(0, 1)$   
 582 than along the diagonal  $\mathbf{q} = |\mathbf{q}|(1, 1)/\sqrt{2}$ . Physically, this implies that dispersion is  
 583 slower along the axis than along the diagonal. This can be understood by considering  
 584 the streamline geometry: continued advection along one of the axes requires particles to  
 585 also meander in the perpendicular direction, resulting in a decrease in average speed by  
 586 a factor  $1/2$ ; by contrast, advection along the diagonal happens in staircase-like fashion  
 587 which decreases the speed by a factor  $1/\sqrt{2}$ . That motion along the diagonal is faster is  
 588 also apparent in the rate function  $g(\xi)$  obtained by Legendre transform and shown on the  
 589 right panel of Figure 6: when  $|\xi|$  is not small, the contours of  $g$ , which directly correspond  
 590 to concentration contours, are anisotropic with the larger scalar concentrations along the  
 591 diagonal.

592 A direct Monte Carlo estimate of  $g$  — as opposed to the indirect estimate deduced from  
 593 Legendre transforming the Monte Carlo approximation to  $f$  — proves difficult to compute  
 594 reliably. Figure 7 illustrates this: even for a large number of realisations of  $4 \times 10^7$ , the  
 595 direct Monte Carlo approach only provides a valid approximation for  $|\xi| \lesssim 2.5$ , in range

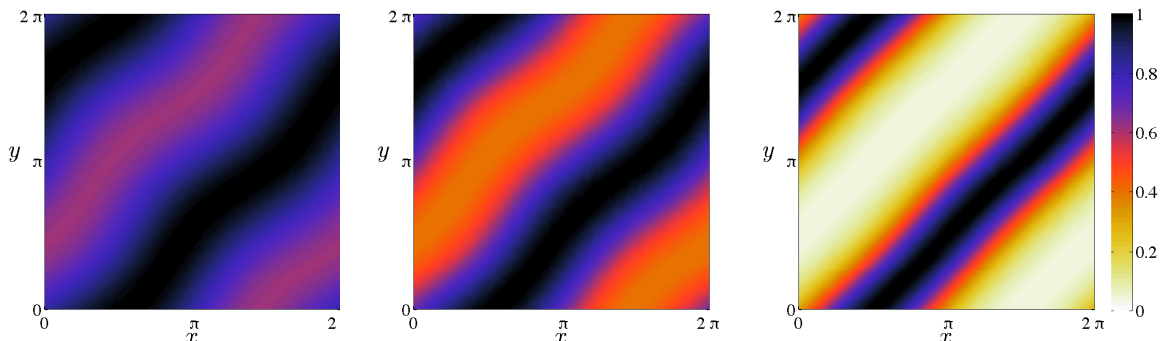


FIGURE 8. (Colour online.) Eigenfunctions for  $Pe = 1$  and  $q_1 = q_2 = 0.5$  (left), 1 (middle) and 5 (right). The eigenfunctions have been normalised to have maximum value 1 and plotted using the same colour scale shown on the right.

596 where  $g$  remains roughly isotropic. Attempts at implementing importance sampling in  
 597 a manner analogous to that used for shear flows and described in Appendix B.2 did  
 598 not lead to significant improvements in the estimation of  $g$  in this direct manner. A  
 599 conclusion, therefore, is that a more efficient Monte Carlo approximation to  $g$  is achieved  
 600 by sampling  $f$  and taking a Legendre transform. Of course, for this problem the most  
 601 efficient method for obtaining  $f$  and  $g$  remains the numerical solution of the eigenvalue  
 602 problem (2.8).

603 It is interesting to examine the eigenfunctions  $\phi$  associated with the eigenvalue  $f(\mathbf{q})$  for  
 604 given  $\mathbf{q}$  since these provide the structure of the scalar field at position  $\boldsymbol{\xi}t = \nabla_{\mathbf{q}}f(\mathbf{q})t$  (with  
 605  $f$  convex so that  $\mathbf{q}$  can be interpreted as a proxy for  $\boldsymbol{\xi}$ ). Figure 8 shows the eigenfunctions  
 606 obtained by numerical solution of the eigenvalue problem for three values of  $q_1 = q_2 =$   
 607  $|\mathbf{q}|/\sqrt{2}$ . For small  $|\mathbf{q}|$  and hence small  $|\boldsymbol{\xi}|$ ,  $\phi$  is essentially constant over the whole cell,  
 608 with only small modulations. This is consistent with the perturbative treatment of the  
 609 eigenvalue problems for  $|\mathbf{q}| \ll 1$  and  $|\boldsymbol{\xi}| \ll 1$ , amounting to homogenisation, which  
 610 indicates that  $\phi = 1 + O(|\mathbf{q}|)$ . As  $|\mathbf{q}|$  and  $|\boldsymbol{\xi}|$  increase, the modulations, in the form of  
 611 diagonal stripes, increase in amplitude so that, for large  $|\boldsymbol{\xi}|$ ,  $\phi$  is close to zero in wide  
 612 stripes. The form of the eigenfunctions depends on the angle of  $\mathbf{q}$ , of course, and for  
 613  $q_1 = 0$  or  $q_2 = 0$  for instance, corresponding to dispersion along the  $x$  and  $y$  axes, they  
 614 have a cellular rather than banded structure (not shown). The structure of the  
 615 eigenfunctions is consistent with the concentration field shown in Figure 4. To see this,  
 616 recall that the concentration depends on both  $\phi$  and on the rate function  $g$ ; across a single  
 617 cell, the latter varies slowly and can be approximated by a Taylor expansion, leading to  
 618 the spatial dependence  $\phi(\mathbf{x}, \mathbf{q}) \exp(\mathbf{q} \cdot \mathbf{x})$ , since  $\nabla g = \mathbf{q}$ . For large  $|\mathbf{q}|$ , the dominant effect  
 619 is the exponential decay of the concentration in the direction of  $\mathbf{q}$ , with the form of  $\phi$   
 620 introducing the banded modulations observed in Figure 4.

621 Some insight into the large-deviation behaviour of cellular flows can be gained by  
 622 considering the regime  $Pe \ll 1$  corresponding to weak advection. The effective diffusivity  
 623 in this limit was computed by Moffatt (1983, §7) and Sagues & Horsthemke (1986) who  
 624 obtained (in our notation) the approximation  $k = 1 + Pe^2/8 + O(Pe^4)$ . The generalisation  
 625 to the large-deviation regime is straightforward and described in Appendix C. It leads  
 626 to the asymptotic approximation

$$f(\mathbf{q}) = q_1^2 + q_2^2 + \frac{Pe^2}{8} \frac{q_1^2 + q_2^2 + q_1^4 + 6q_1^2q_2^2 + q_2^4}{1 + 2(q_1^2 + q_2^2) + (q_1^2 - q_2^2)^2} + O(Pe^3) \quad (4.2)$$

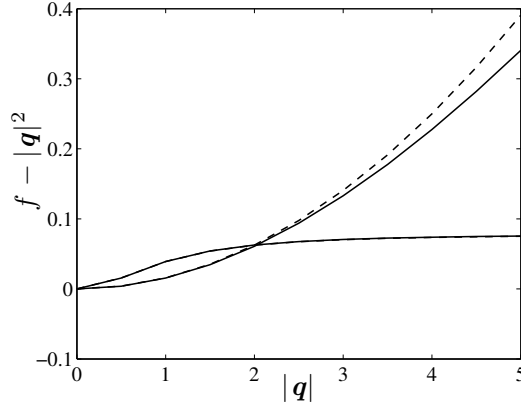


FIGURE 9. Correction  $f - |\mathbf{q}|^2$  as a function of  $|\mathbf{q}|$  for the cellular flow with  $\text{Pe} = 1/4$  and for  $\mathbf{q} = |\mathbf{q}|(1, 1)/\sqrt{2}$  (rapidly growing curves) and  $\mathbf{q} = |\mathbf{q}|(1, 0)$  (other curves, values multiplied by 10). The exact result (solid) is compared with the small-Pe approximation (dashed).

627 whose small- $\mathbf{q}$  limit is consistent with the effective diffusivity just quoted. This ap-  
 628 proximation is tested against numerical results in Figure 9 which shows the correction  
 629  $f(\mathbf{q}) - |\mathbf{q}|^2$  to purely diffusive behaviour for  $\text{Pe} = 1/4$ . The figure confirms the validity  
 630 of (4.2); it also shows that dispersion is fastest along the diagonal, as noted for  $\text{Pe} = 1$ .  
 631 The  $O(\text{Pe}^2)$  correction to  $f$  behaves in fact very differently for  $q_1 = q_2$  than it does for  
 632  $q_1 \neq q_2$ : whereas it is bounded as  $\mathbf{q} \rightarrow \infty$  for  $q_1 \neq q_2$ , it grows quadratically for  $q_1 = q_2$   
 633 in a manner that suggests that (4.2) is not uniformly valid. Eq. (4.2) shows immediately  
 634 that the difference in behaviour stems from the fact that the denominator of the  $O(\text{Pe}^2)$   
 635 term is quadratic for  $q_1 = q_2$  but quartic, like the numerator, otherwise. This is the mani-  
 636 festation of a phenomenon that can be captured by a large- $|\mathbf{q}|$  asymptotic analysis which  
 637 we do not present here. Briefly, this analysis reveals the direction  $q_1 = q_2$  to be singular  
 638 for the flow (4.1) in that the correction to the diffusive behaviour  $f(\mathbf{q}) \sim |\mathbf{q}|^2$  is  $O(|\mathbf{q}|)$   
 639 in this direction while it is  $O(1)$  in all other directions. Flows with more complicated spatial  
 640 structures than (4.1) have other singular directions so that we expect the dependence of  
 641  $f(\mathbf{q})$  on the direction of  $\mathbf{q}$  to be very complicated.

642 We conclude our discussion of cellular flows by briefly considering the large-Pe regime.  
 643 This is the regime that has received most attention in the now extensive literature on  
 644 effective diffusivity for cellular flows. Starting with Childress (1979), several authors have  
 645 applied a boundary-layer analysis to the cell problem of homogenisation to conclude that  
 646  $\mathbf{k} \propto \text{Pe}^{1/2}$  in this case (see Shraiman 1987; Rosenbluth et al. 1987), with Soward (1987)  
 647 deriving an explicit expression for the proportionality constant. Part II of the present  
 648 paper is devoted to a detailed asymptotic treatment of the large-deviation eigenvalue  
 649 problem for  $\text{Pe} \gg 1$  which recovers and extends this result. Here we only discuss some  
 650 qualitative properties of the solution derived numerically.

651 Figure 10 shows  $f$  and  $g$  obtained by numerical solution of the eigenvalue problem  
 652 and Legendre transform for  $\text{Pe} = 250$ . The anisotropy for  $|\mathbf{q}| \gtrsim 1$  observed for  $\text{Pe} = 1$   
 653 is stronger for this large-Pe case: there is a clear suggestion that the contours of  $f(\mathbf{q})$   
 654 tend to straight lines (corresponding to  $f$  being a function of  $|q_1| + |q_2|$ ) for  $|\mathbf{q}| \gg 1$ ;  
 655 correspondingly,  $g(\boldsymbol{\xi})$  depends on  $\max(|\xi_1|, |\xi_2|)$  for  $|\boldsymbol{\xi}| \gg 1$ .

656 The eigenfunctions of (2.8) shown in Figure 11 for three different values of  $q_1 = q_2$   
 657 illustrate different regimes of dispersion that arise at increasingly larger distances from  
 658 the scalar-release point. For small  $|\mathbf{q}|$  and hence for small  $|\boldsymbol{\xi}|$ ,  $\phi$  is almost uniform: a gentle

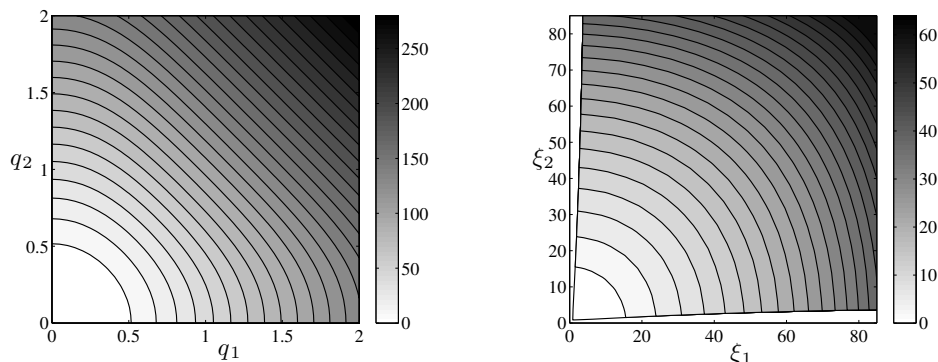


FIGURE 10. Left:  $f$  as a function of  $\mathbf{q}$  obtained by solving the eigenvalue problem (2.8) for the cellular flow with  $Pe = 250$ . Right: rate function  $g$  deduced by Legendre transform.

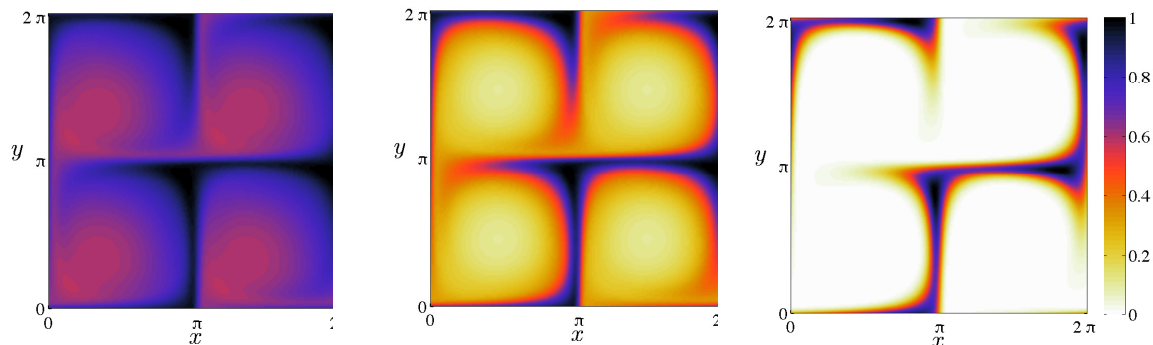


FIGURE 11. (Colour online.) Eigenfunctions for  $Pe = 250$  and  $q_1 = q_2 = 0.1$  (left),  $0.25$  (middle) and  $1$  (right), corresponding to  $\xi_1 = \xi_2 = 4.2, 20.5$  and  $88.1$ . The eigenfunctions have been normalised to have maximum value  $1$  and plotted using the same colour scale shown on the right.

659  $O(|\mathbf{q}|)$  gradient in the cell interiors is compensated by a rapid change in boundary layers  
 660 that appear around the separatrices in agreement with the homogenisation treatment. For  
 661 larger  $\mathbf{q}$  and  $|\boldsymbol{\xi}|$ ,  $\phi$  inside the cell is no longer close to uniform; instead, it is approximately  
 662 constant along streamlines but varies across streamlines, from small values at the centre  
 663 to large values near the separatrices. Again, boundary layers around the separatrices  
 664 ensure periodicity. Finally, for large  $|\mathbf{q}|$  and  $|\boldsymbol{\xi}|$ ,  $\phi$  is close to zero in the cell interiors  
 665 and the scalar is confined within boundary layers. This qualitative description of the  
 666 eigenfunctions is consistent with the evolution of the scalar field shown in Figure 5; it is  
 667 supported by the asymptotics results reported in Part II.

## 668 5. Discussion

669 This paper discusses the statistics of passive scalars or particles dispersing in fluids  
 670 under the combined action of advection and molecular diffusion. It shows how large-  
 671 deviation theory provides an approximation to the scalar concentration or particle-  
 672 position pdf in the large-time limit. This approximation, expressed in terms of the rate  
 673 function  $g(\boldsymbol{\xi})$ , is valid in the tail of the distribution as well as in the core; it considerably  
 674 generalises the more usual diffusive approximation which characterises the dispersion by

675 a single effective-diffusivity tensor. The rate function is deduced from the solution of  
 676 the generalised cell problem (2.8), a one or two-parameter family of eigenvalue problems  
 677 that generalise the cell problem solved when computing the effective diffusivity using the  
 678 method of homogenisation.

679 The application to shear flows reveals features of the dispersion that are not captured  
 680 by the standard theory of shear dispersion initiated by Taylor (1953). In particular, it  
 681 shows that the diffusive approximation dramatically overestimates scalar concentrations  
 682 far away from the centre of mass. The reason for this is that the mechanism underlying  
 683 shear dispersion—the interaction between shear and cross-stream molecular diffusion—  
 684 leads to along-flow dispersion with a finite speed, namely the maximum flow speed.  
 685 The non-zero concentrations beyond the limits imposed by this finite speed are entirely  
 686 attributable to molecular diffusion and thus controlled by molecular rather than effective  
 687 diffusivity.† At intermediate distances from the centre of mass, however, the non-diffusive  
 688 effects can in some cases increase and in some cases decrease dispersion. This can be  
 689 detected in some of the results for standard shear flows displayed in Figure 2 or be  
 690 deduced from the order-by-order corrections to the diffusive approximation discussed in  
 691 §2.3.

692 Our analysis of spatially periodic flows and, in particular, of the classical cellular  
 693 flow further demonstrates the benefits of large-deviation theory over homogenisation and  
 694 the resulting diffusive approximation. The anisotropy of the dispersion in this flow, for  
 695 instance, although a clear consequence of the streamline arrangement, is overlooked by  
 696 the diffusive approximation but quantified by large deviation. As for shear flows, there  
 697 is also a finite speed effect for the dispersion in cellular flow; this is more subtle and is  
 698 elucidated in Part II which devoted to a detailed analysis to the large-Pe limit.

699 The differences between the diffusive and large-deviation approximations for the scalar  
 700 concentration are significant at large enough distances away from the centre of mass of  
 701 the scalar. Since the concentration at such distances is small, large deviation applied to  
 702 problems involving purely passive scalars is of practical importance in situations where  
 703 low concentrations matter, as would be the case, for instance, for very toxic chemicals.  
 704 In such applications the logarithm of the concentration is often a relevant measure of the  
 705 chemical’s impact; it is read off from the rate function since  $\log C \sim -tg(\boldsymbol{\xi})$ . As mentioned  
 706 in §1, for scalars that are reacting, the properties of dispersion at large distances embodied  
 707 in  $g$  can be critical in determining the main features of the scalar distribution. This was  
 708 made explicit in the work of Gärtner & Freidlin (1979) and Freidlin (1985) which relates  
 709 the speed of propagation of fronts for scalars experiencing F-KPP-type reactions to the  
 710 rate function  $g(\boldsymbol{\xi})$  characterising passive dispersion. Following from this relationship, the  
 711 results of the present paper and of Part II can be used to predict front speeds in a range  
 712 of shear and periodic flows. We will report elsewhere the novel predictions that can be  
 713 obtained in this manner (Tzella & Vanneste 2014*a,b*).

714 We conclude by remarking that the large-deviation treatment of scalar dispersion can  
 715 be extended to a class of flows much broader than that considered in the present pa-  
 716 per. Dispersion in time-periodic flows, random flows and turbulent flows can also be  
 717 characterised by a rate function to improve on the approximation provided by effective  
 718 diffusivity. In the time-periodic case an extension of the theory discussed in §2 is straight-  
 719 forward: the eigenfunction  $\phi$  in (2.4) should depend on  $t$  as well as on  $\boldsymbol{x}$  and  $\boldsymbol{\xi}$ , leading

† Molecular diffusion itself, with its infinite propagation speed, is of course only a model for Brownian motion; more sophisticated models with finite propagation speeds such as the telegraph equation can be developed (e.g., Zauderer 2009; see Keller 2004 for connections with large deviations).

720 to an additional term  $\partial_t \phi$  in the eigenvalue problem (2.8) and to the requirement that  
 721  $\phi$  be time periodic which determines the eigenvalue  $f$ . In the random case, under the  
 722 assumption of homogeneous and stationary statistics for  $\mathbf{u}(\mathbf{x}, t)$ ,  $f$  is determined by the  
 723 analogous requirement that  $\phi$ , a random function, be homogeneous and stationary. Im-  
 724 plementing this requirement is not straightforward, however, and Monte Carlo methods  
 725 with importance sampling of the types described in Appendix B may be best suited for  
 726 the computation of the rate function.

727 **Acknowledgments.** JV acknowledges support from grant EP/I028072/1 from the UK  
 728 Engineering and Physical Sciences Research Council.

## 729 Appendix A. Small- $|q|$ expansion for shear flows

730 It follows from the scaled large-deviation form of  $C$  for shear flows (3.2) that

$$\partial_t C \sim (g' \xi - g)C = f(q)C \quad \text{and} \quad \partial_x^n C \sim (-\text{Pe}^{-1} g')^n C = (-\text{Pe}^{-1} q)^n C.$$

731 In these expressions,  $q$  is related to  $\xi = \text{Pe}^{-1} x/t$  by  $\xi = f(q)$  and factors  $1 + O(t^{-1})$   
 732 describing the error in the WKB-like expansion (3.2) are omitted. Thus if we write

$$f(q) \sim \sum_{n=1}^N \alpha_n q^n, \quad (\text{A } 1)$$

733 an equation for  $C$  follows in the form

$$\partial_t C \sim \sum_{n=1}^N (-\text{Pe})^n \alpha_n \partial_x^n C.$$

734 The solution to this equation gives for  $C$  a form similar to (3.2) with  $g$  approximated by  
 735 the Legendre transform of the  $N$ -term Taylor expansion of  $f(q)$  at  $q = 0$ . In particular,  
 736 truncating at  $N = 2$  gives the dispersive approximation with effective diffusivity (2.18).

737 The perturbative solution of (3.4) is straightforward: introducing (A 1) and

$$\phi(y) = 1 + \sum_{n=1}^N q^n \phi_n(y)$$

738 into (3.4) and omitting the term in  $\text{Pe}^{-2}$  gives at the first three orders,

$$\frac{d^2 \phi_1}{dy^2} = \alpha_1 - u, \quad \frac{d^2 \phi_2}{dy^2} = \alpha_2 + \alpha_1 \phi_1 - u \phi_1 \quad \text{and} \quad \frac{d^2 \phi_3}{dy^2} = \alpha_3 + \alpha_2 \phi_1 + \alpha_1 \phi_2 - u \phi_2. \quad (\text{A } 2)$$

739 Integrating the first equation and using (3.1) gives  $\alpha_1 = 0$  and

$$\frac{d\phi_1}{dy} = - \int_{-1}^y u(y') dy'. \quad (\text{A } 3)$$

740 An explicit expression for  $\phi_1$  follows, which can be chosen such that  $\langle \phi_1 \rangle = 0$ . Integrating  
 741 the second equation in (A 2) and using the above gives

$$\alpha_2 = \langle u \phi_1 \rangle = \left\langle \left( \int_{-1}^y u(y') dy' \right)^2 \right\rangle. \quad (\text{A } 4)$$

742 Up to the factor  $\text{Pe}^2$ , this is the effective diffusivity of Taylor and homogenisation theory.  
 743 The function  $\phi_2(y)$  can then be computed explicitly and the condition  $\langle \phi_2 \rangle = 0$  imposed.



744 Finally, integrating the third equation in (A 2) gives

$$\alpha_3 = \langle u\phi_2 \rangle = \langle u\phi_1^2 \rangle, \quad (\text{A } 5)$$

745 in agreement with Young & Jones (1991). Note that the analogue of (A 4) for pipe flows  
746 is

$$\alpha_2 = 2 \int_0^1 \left( \int_0^r r' u(r') dr' \right)^2 \frac{dr}{r}. \quad (\text{A } 6)$$

## 747 Appendix B. Monte Carlo computations

### 748 B.1. Resampled Monte Carlo

749 We test the theoretical results by estimating the cumulant generating function from  
750 Monte Carlo simulations. This relies on solving (2.2) for an ensemble of trajectories  
751  $\mathbf{X}^{(k)}$ ,  $k = 1, \dots, K$ , then computing

$$W_K(t) = \frac{1}{K} \sum_{k=1}^K w^{(k)}(t), \quad \text{where } w^{(k)}(t) = e^{\mathbf{q} \cdot \mathbf{X}^{(k)}(t)}, \quad (\text{B } 1)$$

752 for fixed  $\mathbf{q}$ . Since  $W_K(t) \rightarrow \mathbb{E} \exp(\mathbf{q} \cdot \mathbf{X})$  as  $K \rightarrow \infty$ ,  $f(\mathbf{q}) \approx t^{-1} \log W_K(t)$  for  $t$  and  $K$   
753 large.

754 When  $\mathbf{q}$  is small, this method provides a good estimate of  $f(\mathbf{q})$  with  $t$  moderately  
755 large, say  $t = 5$  or  $10$ . For  $\mathbf{q}$  of order one or large, obtaining even a crude estimate of  
756  $f(\mathbf{q})$  requires an exceedingly large number of realisations  $K$ . This is because the cumulant  
757 generating function is determined by exponentially rare, hence difficult to sample, realisa-  
758 tions whose weights  $w^{(k)}(t)$  are exponentially larger than those of typical realisations. To  
759 estimate  $f(\mathbf{q})$  accurately with a reasonable number of realisations, it is necessary to use  
760 an importance-sampling method which concentrates the computational efforts on reali-  
761 sations that dominate (B 1). We have adopted a simple method based on Grassberger's  
762 (1997) pruning-and-cloning technique (see also Grassberger 2002; Tailleur & Kurchan  
763 2007; Vanneste 2010) which we now describe.

764 Every few time steps in the numerical integration of (2.2), the current weight  $w^{(k)}(t)$   
765 of each realisation is compared to the average  $W_K(t)$ . If  $w^{(k)}(t) > PW_K(t)$ , where  $P >$   
766  $1$  is a parameter of the method (typically chosen as  $P = 2$  or  $3$ ), the realisation is  
767 cloned: an additional realisation  $\mathbf{X}^{(l)}$  is created and integrated forward from the initial  
768 condition  $\mathbf{X}^{(l)}(t) = \mathbf{X}^{(k)}(t)$ . The two clones subsequently follow different trajectories,  
769  $\mathbf{X}^{(l)}(t') \neq \mathbf{X}^{(k)}(t')$  for  $t' > t$  because they experience different Brownian motions. The  
770 statistics of  $W_K(t)$  are left unchanged provided that the weight of the cloned realisations  
771 is divided by 2, that is, the weights  $w^{(k)}(t)$  in (B 1) are multiplied by additional factors  
772 of  $1/2$  for each cloning experienced by realisation  $k$ . If  $w^{(k)}(t) < W_K(t)/P$ , on the other  
773 hand, the realisation is pruned: it is killed with probability  $1/2$  and, if surviving, its  
774 weight  $w^{(k)}(t)$  is multiplied by 2. To keep the number of realisations  $K$  constant, random  
775 realisations are either cloned or killed. We have implemented a slight extension of the  
776 method described in which the number of clones for realisations with  $w^{(k)}(t) > PW_K(t)$ ,  
777 is  $\lfloor w^{(k)}(t)/W_K(t) \rfloor + 1$ .

778 The resampling steps make the method very efficient, and the results reported in the  
779 paper typically required a few minutes of computation on a modest desktop computer.  
780 Crucial to this efficiency is the fact that the cloning-pruning process tailors the ensemble  
781 of realisations to a particular value of  $\mathbf{q}$  by selecting those which dominate  $\mathbb{E} \exp(\mathbf{q} \cdot \mathbf{X})$ .

## B.2. Modified dynamics

The rate function  $g$  can be estimated directly by Monte Carlo simulations, using a binning procedure to approximate  $C$ . This is of course highly inefficient for the parts of  $g$  away from its minimum  $\xi_*$  since these are controlled by exponentially rare realisations which are poorly sampled. One way of remedying this is to integrate a modified dynamics following the importance-sampling technique discussed in Milstein (1995). For shear flows, we have adopted the following approach. The modified dynamics, denoted by tilde, is given by

$$d\tilde{X} = \text{Pe} u(\tilde{Y})dt + \sqrt{2}dW_1, \quad d\tilde{Y} = r(\tilde{Y})dt + \sqrt{2}dW_2, \quad (\text{B } 2)$$

instead of (3.6). Here  $r(y)$  is a function chosen so that the distribution of  $\tilde{Y}$  better samples the regions where  $u(y)$  is large (or small) which control  $g(\xi)$  for  $\xi$  away from  $\xi_*$ . Girsanov's formula relates averages under the original dynamics (2.2) to averages under this modified dynamics according to

$$\mathbb{E} \cdot = \tilde{\mathbb{E}} \cdot e^{-\frac{1}{\sqrt{2}} \int_0^t r(\tilde{Y}(t')) dW_2 - \frac{1}{4} \int_0^t r^2(\tilde{Y}(t')) dt'}$$

(Milstein 1995; Øksendal 1998). Thus  $C(x, t)$  can be approximated by integrating numerically (B 2) for an ensemble of trajectories and using a discretised version of the relation

$$C(x, t) = \tilde{\mathbb{E}} \delta(x - \tilde{X}(t)) e^{-\frac{1}{\sqrt{2}} \int_0^t r(\tilde{Y}(t')) dW_2 - \frac{1}{4} \int_0^t r^2(\tilde{Y}(t')) dt'}$$

This result is used for to estimate the tails of  $C$  and hence the form of  $g$  for large  $|\xi|$  with a much better sampling than achieved with the original dynamics. For the numerical results reported in §3.1–3.2, we have used  $r(y) = \gamma(1 - y)$  to efficiently sample the portion of  $C(x, t)$  controlled by trajectories that remain localised near the wall at  $y = 1$  (leading to anomalously large  $x$  for Couette flow and anomalously small  $x$  for Poiseuille flow), and  $r(y) = -\gamma y$  to sample trajectories localised near the maximum of the plane Poiseuille flow. The value of the parameter  $\gamma$  was chosen by trial-and-error to obtain the best representation of a portion of the curve  $g(\xi)$ . A similar modified dynamics for both  $Y(t)$  and  $Z(t)$  was used in the case of the pipe Poiseuille flow in §3.3.

Appendix C. Small-Pe form of  $f(q)$  for cellular flow

In the limit  $\text{Pe} \rightarrow 0$ , the eigenvalue problem (2.8) can be solved perturbatively by introducing the expansions

$$\phi = \phi_0 + \text{Pe}\phi_1 + \text{Pe}^2\phi_2 + \dots \quad \text{and} \quad f = f_0 + \text{Pe}f_1 + \text{Pe}^2f_2 + \dots$$

of the eigenfunctions and eigenvalue into (2.8). The leading-order,  $O(1)$ , equation is solved for  $\phi_0 = 1$  and  $f_0 = |\mathbf{q}|^2$  which reduces the  $O(\text{Pe})$  equation to

$$\nabla^2 \phi_1 - 2\mathbf{q} \cdot \nabla \phi_1 + \mathbf{u} \cdot \mathbf{q} = f_1.$$

On integrating over a period, the left-hand side vanishes, leading to  $f_1 = 0$ . The solution is then found in the form

$$\phi_1 = a \sin x \sin y + b \sin x \cos y + c \cos x \sin y + d \cos x \cos y, \quad (\text{C } 1)$$

where the constants  $a$ ,  $b$ ,  $c$  and  $d$  are readily computed. Integrating the  $O(\text{Pe}^2)$  equation

$$\nabla^2 \phi_2 - 2\mathbf{q} \cdot \nabla \phi_2 - \mathbf{u} \cdot \nabla \phi_1 + \mathbf{u} \cdot \mathbf{q} \phi_1 = f_2$$

814 over a period leads to the eigenvalue correction

$$f_2 = \frac{1}{(2\pi)^2} \int_0^{2\pi} \int_0^{2\pi} (-\mathbf{u} \cdot \nabla \phi_1 + \mathbf{u} \cdot \mathbf{q} \phi_1) \, dx dy.$$

815 Substituting (C 1) and taking the explicit form of the constants into account yields

$$f_2 = \frac{1}{8} \frac{q_1^2 + q_2^2 + q_1^4 + 6q_1^2 q_2^2 + q_2^4}{1 + 2(q_1^2 + q_2^2) + (q_1^2 - q_2^2)^2}. \quad (\text{C } 2)$$

#### REFERENCES

- 816 Aris, R. 1956, On the dispersion of a solute in a fluid flowing through a tube, *Proc. R. Soc.*  
 817 *Lond. A* **235**, 67–76.
- 818 Bensoussan, A., Lions, J. L. & Papanicolaou, G. C. 1989, *Asymptotic analysis of periodic struc-*  
 819 *tures*, Kluwer.
- 820 Berestycki, H., Nirenberg, L. & Varadhan, S. R. S. 1994, The principal eigenvalue and maximum  
 821 principle for second-order elliptic operators in general domains, *Comm. Pure Appl. Math.*  
 822 **47**, 47–92.
- 823 Camassa, R., Lin, Z. & McLaughlin, R. M. 2010, The exact solution of the scalar variance in  
 824 pipe and channel flow, *Commun. Math. Sci.* **8**, 601–626.
- 825 Chatwin, P. C. 1970, The approach to normality of the concentration distribution of a solute  
 826 flowing along a straight pipe, *J. Fluid Mech.* **43**, 321–352.
- 827 Chatwin, P. C. 1972, The cumulants of the distribution of concentration of a solute dispersing  
 828 in solvent flowing through a tube, *J. Fluid Mech.* **51**, 63–67.
- 829 Childress, S. 1979, Alpha-effect in flux ropes and sheets, *Phys. Earth Planet. Int.* **20**, 172–180.
- 830 Dembo, A. & Zeitouni, O. 1998, *Large deviations: techniques and applications*, Springer.
- 831 den Hollander, F. 2000, *Large deviations*, Fields Institute Monographs, American Mathematical  
 832 Society.
- 833 Ellis, R. S. 1995, An overview of the theory of large deviations and applications to statistical  
 834 physics, *Actuarial J.* **1**, 97–142.
- 835 Freidlin, M. 1985, *Functional integration and partial differential equations*, Princeton University  
 836 Press.
- 837 Freidlin, M. & Wentzell, A. 2012, *Random perturbations of dynamical systems*, 3rd edn, Springer.
- 838 Gardiner, C. W. 2004, *Handbook of stochastic methods*, 3rd edn, Springer-Verlag.
- 839 Gärtner, J. & Freidlin, M. I. 1979, The propagation of concentration waves in periodic and  
 840 random media, *Soviet Math. Dokl.* **20**, 1282–1286.
- 841 Gorb, Y., Nam, D. & Novikov, A. 2011, Numerical simulations of diffusion in cellular flows at  
 842 high Péclet number, *Discrete Contin. Dyn. Syst. Ser. B* **15**, 75–92.
- 843 Grassberger, P. 1997, Prune-enriched Rosenbluth method: simulations of  $\theta$  polymers of chains  
 844 length up to 1 000 000, *Phys. Rev. E* **56**, 3682–3693.
- 845 Grassberger, P. 2002, Go with the winners: a general Monte Carlo strategy, *Comp. Phys. Comm.*  
 846 **147**, 64–70.
- 847 Haynes, P. H. & Vanneste, J. 2014, Dispersion in the large-deviation regime. Part II: cellular  
 848 flow at large Péclet number, *J. Fluid Mech.* In press. Referred to as Part II.
- 849 Jansons, K. M. & Rogers, L. C. G. 1995, Probability and dispersion theory, *IMA J. Appl. Maths.*  
 850 **55**, 149–162.
- 851 Keller, J. B. 2004, Diffusion at finite speed and random walks, *Proc. Natl. Acad. Sci. USA*  
 852 **101**, 1120–1122.
- 853 Kuske, R. & Keller, J. B. 1997, Large deviation theory for stochastic difference equations, *Euro.*  
 854 *J. Appl. Math.* **8**, 567–580.
- 855 Majda, A. J. & Kramer, P. R. 1999, Simplified models for turbulent diffusion: theory, numerical  
 856 modelling and physical phenomena, *Phys. Rep.* **314**, 237–574.
- 857 Mercer, G. N. & Roberts, A. J. 1990, A centre manifold description of contaminant dispersion  
 858 in channels with varying flow properties, *SIAM J. Appl. Maths.* **50**, 1547–1565.
- 859 Milstein, G. N. 1995, *Numerical solution of stochastic differential equations*, Kluwer.

- 860 Moffatt, H. K. 1983, Transport effects associated with turbulence with particular attention to  
861 the influence of helicity, *Rep. Prog. Phys.* **46**, 621–664.
- 862 Novikov, A., Papanicolaou, G. & Ryzhik, L. 2005, Boundary layers for cellular flows at high  
863 Péclet numbers, *Comm. Pure Appl. Math.* **867–922**, 563–580.
- 864 Øksendal, B. 1998, *Stochastic differential equations*, Springer–Verlag.
- 865 Papanicolaou, G. C. 1995, Diffusion in random media, in J. P. Keller, ed., *Surveys in Applied*  
866 *Mathematics*, Vol. 1, Plenum, pp. 205–253.
- 867 Pavliotis, G. A. & Stuart, A. M. 2007, *Multiscale Methods: Averaging and Homogenization*,  
868 Springer–Verlag.
- 869 Rosenbluth, M. N., Berk, H. L., Doxas, I. & Horton, W. 1987, Effective diffusion in laminar  
870 convective flows, *Phys. Fluids* **30**, 2636–2647.
- 871 Sagues, F. & Horsthemke, W. 1986, Diffusive transport in spatially periodic hydrodynamic flows,  
872 *Phys. Rev. A* **34**, 4136–4143.
- 873 Shraiman, B. I. 1987, Diffusive transport in a Rayleigh–Bénard convection cell, *Phys. Rev. A*  
874 **36**, 261–267.
- 875 Simon, B. 1983, Semiclassical analysis of low lying eigenvalues. I. Non-degenerate minima:  
876 asymptotic expansions, *Ann. Inst. Henri Poincaré* **38**, 295–307.
- 877 Soward, A. M. 1987, Fast dynamo action in a steady flow, *J. Fluid Mech.* **180**, 267–295.
- 878 Tailleur, J. & Kurchan, J. 2007, Probing rare physical trajectories with Lyapunov-weighted  
879 dynamics, *Nature Phys.* **3**, 203–207.
- 880 Taylor, G. I. 1953, Dispersion of soluble matter in solvent flowing slowly through a tube, *Proc.*  
881 *R. Soc. Lond. A* **219**, 186–203.
- 882 Touchette, H. 2009, Large deviation approach to statistical mechanics, *Phys. Rep.* **478**, 1–69.
- 883 Tzella, A. & Vanneste, J. 2014a, Front propagation in cellular flows: a large-deviation approach.  
884 In preparation.
- 885 Tzella, A. & Vanneste, J. 2014b, Front propagation in cellular flows for fast reaction and small  
886 diffusivity. In preparation.
- 887 Vanneste, J. 2010, Estimating generalized Lyapunov exponents for products of random matrices,  
888 *Phys. Rev. E* **81**, 036701.
- 889 Xin, J. 2009, *An introduction to fronts in random media*, Springer.
- 890 Young, W. R. & Jones, S. 1991, Shear dispersion, *Phys. Fluids* **A3**, 1087–1101.
- 891 Zauderer, E. 2009, *Partial differential equations of applied mathematics*, 3rd edn, John Wiley &  
892 Sons.